

SLAC – PUB – 4311
April 1987
(E)

DESIGN, CONSTRUCTION, PROTOTYPE
TESTS AND PERFORMANCE OF A VERTEX
CHAMBER FOR THE MAC DETECTOR*

W. W. Ash, H. R. Band, E. D. Bloom, M. Bosman,^[a] T. Camporesi,^[b]
G. B. Chadwick, M. C. Delfino,^[c] R. De Sangro, W. T. Ford, M. W. Gettner,
G. P. Goderre,^[d] G. L. Godfrey, D. E. Groom, R. B. Hurst, J. R. Johnson,
K. H. Lau, T. L. Lavine, R. E. Leedy, I. Lippi,^[e] T. Maruyama, R. L. Messner,
J. H. Moromisato, L. J. Moss, F. Muller,^[b] H. N. Nelson, I. Peruzzi,
M. Piccolo, R. Prepost, J. Pyrlík, N. Qi, A. L. Read, Jr.,^[f] D. M. Ritson,
L. J. Rosenberg,^[g] W. D. Shambroom,^[h] J. C. Sleeman, J. G. Smith,
J. P. Venuti, P. G. Verdini, E. von Goeler, H. B. Wald, R. Weinstein,
D. E. Wiser, and R. W. Zdarko

Department of Physics, University of Colorado, Boulder, Colorado 80309

I. N. F. N., Laboratori Nazionali di Frascati, Frascati, Italy

Department of Physics, University of Houston, Houston, Texas 77004

Department of Physics, Northeastern University, Boston, Massachusetts 02115

Department of Physics and Stanford Linear Accelerator Center,

Stanford University, Stanford, California 94305

Department of Physics, University of Utah, Salt Lake City, Utah 84112

Department of Physics, University of Wisconsin, Madison, Wisconsin 53706

Submitted to *Nuclear Instruments and Methods*

* This work was supported in part by the U. S. Department of Energy under contract numbers DE-AC02-81ER40025 (CU), DE-AC03-76SF00515 (SLAC), and DE-AC02-76ER00881 (UW); by the National Science Foundation under grant numbers NSF-PHY82-15133 (UH), NSF-PHY82-15413 and NSF-PHY82-15414 (NU), and NSF-PHY83-08135 (UU); and by the Istituto Nazionale di Fisica Nucleare.

ABSTRACT

The design considerations, construction techniques, prototype tests and performance characteristics, of a pressurized drift chamber used in the MAC detector at PEP are described. The chamber consists of 324 aluminized mylar tubes of 6.9 mm diameter with wall thickness of $100\mu\text{m}$. With appropriate shielding it operates successfully at 4.6 cm from the beam line. It was simple to construct and was configured to permit any malfunctioning tubes to be remotely disconnected without affecting operation.

The chamber operated without problems for two years in the PEP environment with a gas mixture of 49.5% Argon, 49.5% CO_2 , 1% CH_4 , at 4 atm absolute pressure. The mean spatial resolution averaged over all tubes was $45\mu\text{m}$. The time to distance relation for this gas mixture, along with the geometric positioning of individual wires relative to the central tracking chamber, was obtained with data from Bhabha scattering events.

We also describe resolution studies performed with a prototype chamber, in a SLAC test beam. A wide range of gases, gas pressures, and electronic parameters were explored. These studies proved that resolutions in the $10\text{-}50\mu\text{m}$ range were possible.

Our experience demonstrates that chambers of this type provide high precision tracking and are particularly suited for operation in regions with difficult physical access and/or high ambient radiation levels.

1. Introduction

The measurement of a comparatively long lifetime associated with particles containing b-quarks provided the motivation to upgrade the tracking capability of the PEP detector MAC with a Vertex Chamber (VC) of sufficient precision to measure particle flight paths of less than 1 mm. Originally, the MAC detector relied on a Central Drift (CD) Chamber with a spatial resolution of about 180–200 μ m and with the first layer of wires placed at a radius of 12 cm.

The objective of the upgrade was to add a high precision vertex chamber without modifying the existing tracking chamber. There was no space between the CD and the existing beam pipe, so the device had to be placed much closer to the circulating beams of an e^+e^- storage ring than had previously been attempted. Shielding studies led us to believe that this was feasible and indeed the observed radiation levels were close to expectations.

The detector had to be capable of operating in a region difficult to access and with high ambient radiation levels. Less than one year was available for production of a fully operational chamber, including prototype and design studies. This ruled out the use of solid state or other new technologies. Because good wire chamber lifetimes have been obtained with flat cathodes,^[1] as opposed to wire configurations, and since a broken wire would be contained within a tube, we were led to consider a “straw chamber” (*i.e.* a chamber of small diameter mylar tubes wire tubes) adapted from the HRS collaboration design.^[2] Further considerations, described here, convinced us of the excellence of this design.

Monte Carlo and analytical studies^[3] based on the programs and work of Vavra,^[4] Jaros,^[5] Boyarsky,^[6] and others, provide general guidelines for obtaining high resolution with drift chambers. Briefly they can be summarized as follows:

- (a) The fluctuation in spacing between ionization clusters, not diffusion, provides the dominant contribution to spatial resolution for drift distances < 1 mm. Use of high gas pressure reduces this contribution, and also reduces the effect of diffusion for larger drift distances.
- (b) For all drift distances < 3.5 mm, timing on the first electron to arrive at the sense wire affords the best spatial resolution. To insure one's capability to trigger on the first electron, one should maintain the ability to operate at high gas gain, strive for the least crosstalk between neighboring channels, and use the best possible electronic signal processing.

Potential problems of small drift tubes are:

- (a) The variable electric field, which leads in some gases a drift velocity that is not constant as a function of drift distance.

- (b) Imperfect axial alignment of the tube wall, which can cause an electrostatic force on the sense wire that moves the wire off the tube axis for high voltages.
- (c) Loss of resolution near the wire, which occurs in all drift chambers, but degrades a larger fraction of the sensitive area in a small cell device.

As described below these problems were in large measure overcome and did not limit operation.

The advantages of the technique are:

- (a) Chamber construction with tubes is simple. Each tube can be independently tested in place and the chamber can be designed so that any malfunctioning tube may be separately disconnected without affecting overall operation of the system.
- (b) The tube configuration provides a large cathode area and minimizes cathode associated problems. It further functions as a cylindrical transmission line which is well shielded against crosstalk between neighboring elements, especially if it is terminated with its characteristic impedance.
- (c) The cylindrical geometry gives optimal collection for timing off the first arriving electron.
- (d) Since all cells are identical, calibrations are easy to perform.

In the following sections we describe our program of design, construction, testing and data handling for the chamber, emphasizing those aspects that we believe will be useful to others engaged in similar work. We first discuss the radiation shielding used, since it was an essential ingredient in the success of the chamber operation, then we give the final design of the chamber itself. Next we present construction details and describe the electronics and gas handling equipment. After these are discussed, we describe the results of tests which were performed with a prototype setup, and present data obtained for gas mixtures and conditions not used in the final experimental situation.

The final section of the paper describes the performance of the actual chamber during two years of operation and the software techniques used to obtain the time to distance relationship and find cell by cell calibrations. The pattern recognition techniques are described, and finally the measured spatial resolutions are presented.

2. Shielding Design

Early in the operation of the MAC detector, the original, conservative beam pipe was damaged. Time constraints forced the use of a temporary beam pipe of only 3.15 cm radius and minimal shielding. We observed that under these conditions backgrounds were highly dependent on steering and on beam quality. When the beam was well tuned, the number of background hits in the central tracking chamber was surprisingly small and did not appreciably degrade pattern recognition. However the background caused extra DC current to be drawn by the chamber; surges in the background induced large currents via the Malter effect. This was unacceptable for long term operation of the CD or the proposed Vertex Chamber.

We deduced that the main background came from beam particles that had lost substantial energy by bremsstrahlung in the straight sections of PEP and then were overfocussed by the low-beta quadrupoles near to the Interaction Region (IR). These electrons and positrons struck the vacuum pipe and initiated showers in the vicinity of the tracking chamber. Some background came from synchrotron radiation as well. We estimated that these backgrounds had to be suppressed by at least an order of magnitude. To achieve this reduction we formulated and imposed three conservative design criteria, criteria that had to apply over the allowed range of beam steering parameters:

- (a) The beam pipe in the neighborhood of the Vertex and Central Drift Chambers should be geometrically shadowed by nearby collimators from overfocussed electrons. We refer to these collimators as the 'close-in' collimators. Additional shielding had to be placed around these collimators to absorb the electromagnetic showers before they entered the tracking chambers.
- (b) The close-in collimators should also geometrically shadow the VC from synchrotron radiation produced as the beam passed through the low-beta quadrupole nearest to the IR, and the next nearest PEP magnet.
- (c) Electrons that had undergone Coulomb scattering by the residual gas in the vacuum chamber ahead of the IR, causing them to be off axis, should be intercepted by existing distant collimators prior to hitting the close-in collimators.

With the aid of beam tracking computer programs, the minimum radii for the close-in collimators consistent with (c) were determined for various distances of these collimators from the IR. The minimum beam pipe radius consistent with both (a) and (b) was then calculated for each of these cases. The distance of the close-in collimators that minimized the beam pipe radius but allowed for adequate shielding between these collimators and the tracking chambers was chosen.

We chose Beryllium for our beam pipe material to reduce multiple scattering. However, we added a $75\mu\text{m}$ cylindrical titanium liner^[7] inside our beam pipe to absorb the secondary fluorescent X-rays generated when the harder synchrotron X-rays struck the close-in collimators. Beryllium is essentially transparent to these X-rays.

Figure 1 shows the final optimized configuration. The beam pipe is 3.6 cm inner diameter; the close-in tantalum collimators are 60 cm from the IR at a radius of 2.8 cm. Surrounding them is a layer of heavimet, a sintered tungsten material, intended to absorb showers initiated by overfocussed electrons in the collimators. The titanium liner placement is also shown.

With this configuration the main source of background was synchrotron X-rays in the energy range of 10-100 keV that were generated in the low-beta quadrupoles by beam halo, then Compton back scattered from the close-in collimators into the VC. The beam halo was fed both by Coulomb scattering in the residual gas of the machine vacuum and by beam-beam interactions. It was much larger than would be estimated from the Gaussian beam spread caused by quantum fluctuations in the emission of synchrotron radiation.

The average observed backgrounds were consistent with the conversion of two 25 keV photons in the VC per beam crossing. This background was relatively insensitive to beam conditions and steering.

3. Chamber and Shielding Mounting

The Vertex Chamber and shielding were mounted on a 1.8 m segment of beam pipe that was physically self supporting, and flanged at either end for connection to the PEP vacuum system. Two radial I-beams, or 'strong-backs', supported the structure between the flanges and the chamber's pressure vessel. The pressure vessel consisted of the Beryllium beam pipe, endplates, and an outer cylindrical aluminum wall. The outer wall provided structural support. Once assembled, the chamber was inaccessible.

The pressure vessel was entirely distinct from the Vertex Chamber itself. The gas inlet and outlet were on either endplate. Gas was supplied through 0.64 mm Poly-flo plastic tubing. Each VC cell was connected to a separate coaxial cable that transmitted its signal. Half of these cables were lead out through each pressure vessel endplate. The cables were bundled together and vacuum cast into cylindrical epoxy plugs, which were sealed with O-rings in the endplates. Four bundles were led through each endplate.

The heavimet shielding occluded existing small angle veto chambers that were important in the MAC search for $e^+e^- \rightarrow \gamma + \text{weakly interacting particles}$.

To maintain veto capability to within 4.5° of the beam, we installed compact detectors consisting of bismuth germanate oxide (BGO) crystals (Figure 1). These were read out by photodiodes that were small and capable of operating in our axial magnetic field. The successful operation of the BGO with photodiode readout marked the first application of this technology in a collider experiment. Both the heavimet and the BGO were strapped to the beam pipe assembly, which supported their weight.

The final system was rugged and trouble free. Disassembly proved unnecessary because no malfunctions occurred.

4. Design and Construction of the Vertex Chamber

4.1 DESIGN

The Vertex Chamber was designed as a 'spool,' consisting of two aluminum endplates epoxied to either end of an extruded Beryllium tube. The straws and wires were then strung between the endplates. The radial pattern of the straws in the endplate is shown in Figure 2. There are six radial layers, arranged in three pairs. The inner member of each pair is close packed in azimuth. We took care that the sense wires of the inner members of the three pairs never align in azimuth. The outer member of each pair is staggered one half cell with respect to the inner member, to allow resolution of the ambiguity of which side of the sense wire a track passed. There are 40 straws in the first layer pair, 54 in the second, and 68 in the third. The endplates were 1.59 mm thick; the holes in them were drilled by a computer controlled milling machine, and were placed with an accuracy of $< 13 \mu\text{m}$.

In Table 1, we give an inventory of matter in the Vertex Chamber and beam pipe assembly. There was 0.8% of a radiation length between the IR and the inner VC layer, for particles exiting at 90° with respect to the beam.

4.2 CONSTRUCTION

The straws obtained commercially.^[8] consisted of two layers of $50 \mu\text{m}$ aluminized mylar, cut in 1.1 cm strips, and wound spirally at a pitch angle of 28° on a mandrel of diameter 6.9 mm. The surface resistivity of the aluminum coating was $0.8 \Omega/\text{square}$; only the external mylar faces were coated. The layers were held together with contact cement. The tubes delivered by the manufacturer had remarkably uniform tolerances. Their inner diameters were the same to within $10 \mu\text{m}$ and they were straight to within $100 \mu\text{m}$. Some were scraped on the inside, breaking the electrical continuity of the inner face. We selected the best straws, then cut them to 432 mm lengths.

The end fittings were then attached to the straw ends. Figure 3 shows the details of one fitting. An aluminum collar was glued with conductive epoxy to the straw inner face, trapping a Delrin (acetal) plastic plug. The plug performed several functions. First, it insulated the high voltage on the sense wire from the ground of the endplate and straws. For this reason, virgin Delrin, that is Delrin that was not reformed from old pieces, was used, to avoid cracks and crevices that lead to high voltage breakdown. Considerable trial and error led to the shape of the plug inside the straw, which avoided edge breakdown at very high voltages. Second, the plug provided a means to apply tension once the straw was mounted between the endplates. The tip of the plug was threaded. After the tip was pulled through the endplate, a nut was torqued to tense and straighten the straw. Third, the plug provided a seat for the feedthrough that held and positioned the sense wire. Last, the plug provided a conduit for gas flow through the straw, via a channel cut lengthwise on its outer radius.

The straw was then mounted between the endplates. The aluminum collar on one end was pressed directly against the aluminum endplate. On the other end, for gas flow exit, ease of construction, and mechanical relief, a gap was left and a spring provided the electrical ground continuity. 500 g of tension was placed on the straw itself. The $30\ \mu\text{m}$ gold-tungsten sense wire was then drawn through the mounted straw, and a feedthrough passed over one end of the wire. The feedthrough was a 3.23 cm long tube of stainless steel, with a $100\ \mu\text{m}$ inner radius and .1 cm outer radius, used to position and hold the sense wire. The feedthrough was crimped to capture one end of the wire, a second feedthrough was passed over the other end of the wire, and a 100 g weight was attached. The second feedthrough was then positioned and crimped. The wire tension was monitored by measurement of the resonant vibration frequency of the wire, with a simple oscillating current and magnet. Figure 4 shows the chamber under construction.

Approximately 30 tubes a day were mounted and strung with wires. Each evening the entire chamber was placed in a pressure vessel filled with 4 atm 50% Argon, 50% C_2H_6 , and the new cells were checked at a very high voltage, corresponding to the transition between limited streamer formation and continuous discharge. Nearly all the straws operated well at voltages in the proportional regime, but approximately 25% became excessively noisy at the very high voltage. These were replaced; usually a small fleck of Delrin was found on the sense wire.

The completed chamber, with its cabling, was slipped over the Beryllium beam pipe which was then welded to the reducing sections (see Figure 1). Welding in the neighborhood of the plastics in the chamber was done with care to

allow cooling. Finally, the outer pressure vessel wall was slipped over the assembly and welded to the pressure vessel endplates.

4.3 ELECTRONICS

Gas Density and High Voltage Control

The gas system was designed to maintain the gas density as constant as possible while allowing for continuous replacement of the gas in the chamber. Gas from pressurized cylinders entered through Poly-flo tubing to one endplate of the pressure vessel, then exited via a similar line on the other side. The gas was exhausted to the atmosphere through a vacuum pump, which was well filtered from the tubing to the chamber and prevented backstreaming. The rate of flow was controlled by a needle valve placed ahead of the pump. The width of the Fe^{55} spectrum in a test straw in a small pressure vessel on the exhaust line was used to monitor the quality of the exhaust gas, and hence set the flow rate. Replacement of the gas in the Vertex Chamber every two hours proved adequate.

Gas pressure and temperature were monitored by semiconductor sensors in the VC and on the input and output gas lines. The sensors in the chamber suffered a shift in DC behavior when the MAC solenoid was activated, but were otherwise stable and reliable. No degradation of the sensors due to radiation was observed.

The gas pressure was maintained by a mechanical regulator system, placed at the output of the pressurized cylinders. The regulators proved sensitive to temperature gradients, so they were thermally isolated. A dedicated electronic circuit also monitored gas density, and could actively control the system via solenoid valves if the density drifted outside a window of $\pm 0.75\%$. The mechanical system would wander at this level on the time scale of one week, but this was easily controlled by occasional human intervention.

No mechanism for regulating temperature was used. The chamber temperature was kept constant by the cooling system of the MAC solenoid. Effects of heating due to the beam were small.

The VC gas system kept the gas density to within an rms variation of 0.8% over one week. For the gas used in the VC this contributed to position uncertainty by an amount proportional to drift distance. For the maximum drift distance of 3.5 mm the effect was about $14\mu\text{m}$.

High voltage was supplied by externally controlled power supplies. The external controls included interlocks with pressure monitors and current sensors, as well as circuits for slow ramping of the high voltage on the chamber. Typically the chamber operated at 3900 volts, and drew $\sim 20\mu\text{A}$ of DC current.

Electronics for Drift Time Measurement

Figure 5 shows the layout of the Vertex Chamber and associated electronics. One end of each tube was terminated in its characteristic impedance, through a stand-off capacitor, to eliminate the reflected signal, and thereby avoid correlation of the drift time with axial location of the track, and to suppress cross talk. Each straw was directly coupled on the other end to a coaxial cable, which transmitted the signal and provided high voltage. RG179B was chosen for its small diameter (2.8 mm), good high voltage capability, high characteristic impedance (75Ω), and heat resistance. Each cable was decoupled from high voltage with a 1000 pf capacitor, and its signal amplified by a LABEN 5242 preamplifier. The layout of this hybrid is shown in Figure 6. This preamplifier was chosen for its fast rise time and low noise, but in retrospect its properties were not optimized for the low impedance source provided by our cables.

The output of each preamplifier was connected in differential mode through ~ 5 m of twisted pair to our discriminator circuit. Each circuit contained two distinct discriminators, set at different thresholds. The output of the low threshold discriminator was delayed with respect to the other. The output of the circuit was the logical AND of these two discriminators. In this way, pulses smaller than the high threshold did not fire the circuit, allowing rejection of noise and crosstalk, but timing on larger pulses was still taken from the low threshold. The circuit utilized the Plessey SP9687 dual comparator chip which exhibits very fast transition times (~ 1 ns) with little slewing, and operates reliably at a 1.5 mV threshold.

The discriminator outputs provided stop signals to the standard MAC circuit for time interval measurement,^[9] the time to voltage converters (TVCs). In this circuit, a start signal derived from the PEP master oscillator initiated the charging of a capacitor, which was then stopped by the discriminator output. If a MAC trigger was recorded, the voltage on the capacitor was digitized with a bin size of 160 ps. One ADC under the control of a 'scanner' board digitized many TVC circuits and eliminated data from circuits where no stop occurred. In the laboratory this system exhibited < 300 ps resolution.

5. Prototype Tests and Results

We now describe the prototype tests which were made during design, and give results which are applicable to the usage of chambers like that described above. The prototype had 16 straws in a 4 by 4 array. The straws were mounted between two endplates on an aluminum beam with the precision mounting techniques already described. The wire spacing interval was 7.2 mm and the inside straw radius was 3.45 mm. The central wires were 20 μm gold plated tungsten. The prototype was mounted inside a plexiglas tube with endplates capable of withstanding high pressure, and the 16 high voltage coaxial leads from the wires penetrated the endplates through an epoxy plug. A photograph of the prototype appears in Figure 7.

The prototype was run in a SLAC test beam with an 8 GeV/c unseparated negative particle beam produced from a Beryllium target bombarded by electrons from the SLAC linear accelerator. The beam contained roughly equal numbers of pions and electrons. The prototype was placed immediately after the final collimator, where beam divergence was only a few milliradians, and beam size was about 3 mm. A small scintillator was placed in the beam ahead of the pressure vessel to provide the zero time signal. array of straws used in the tests.

The electrical circuitry used for the prototype is shown in Figure 8. The tungsten wires were at positive voltage, while the cathodes were grounded. One end of each straw was terminated through a 100 pf capacitor by a 300 Ω resistor and the other was connected to a total of ~ 5 m of 75 Ω coaxial high voltage cable. This cable was decoupled from the high voltage supply by a 1000 pf capacitor, and ended in a preamplifier and cable driver. The signal was split into two paths, one to a LeCroy 623B discriminator and a LeCroy 2228A Time to Digital Converter (TDC), the other to a LeCroy 2249W Analog to Digital Converter (ADC).

The scintillation counter signal was used as the common start pulse for the TDC's, for the gating of the ADC's and to interrupt an LSI 11/23 computer which read the CAMAC output of the TDC and ADC modules. Data was accumulated with the "Atropos" system programs^[10] developed at SLAC.

An additional test setup used a small "staggered straw" arrangement consisting of a single layer of straws with three spaced as before but with the fourth straw offset vertically by one straw radius. This device was inserted into a small test box that could be evacuated or pressurized. This additional test setup was easy to modify and was used to check the effects of different wire radii on resolution and performance.

5.1 INVESTIGATION OF PROPORTIONAL AND LIMITED STREAMER MODES

As noted in the introduction, an optimal strategy for obtaining best drift time resolution over small drift distances In the actual vertex chamber we used none 49.5% Argon, 49.5% CO₂, 1% CH₄, is to use the arrival time of the first electron^[4] of the ionization cluster. This requires high gas gain and/or high quality preamps to ensure that single electron signals exceed the electronic noise. In the prototype tests we investigated performance both at relatively low gains in the proportional mode, at moderate gains in the saturated proportional mode and at high gains in the limited streamer,^[11] or LS mode. Tests were made with an absolute pressure of between one and 4 atm.

The gases used for the tests were Argon-Ethane in a 50:50 mixture, Argon-Isobutane in 75:25 mixture, and Argon-CO₂ in 75:25 mixture. We were able to observe LS pulse production in all the above gases except for the last. The most stable operation at high gain, *i.e.* best plateau and pulse uniformity, was obtained for the highest pressures.

Ultimately we used none of the gases tested, but chose 49.5% Argon, 49.5% CO₂, 1% CH₄, entirely because of its insensitivity to radiation damage.

We used an Fe⁵⁵ source, with its 5.9 keV X-ray emission from the Manganese K_α transition, to provide a calibration signal. This radiation penetrated the thin straw wall and released ~ 240 electrons in a single cluster. Additionally we used pulses from single electrons produced by photo-emission from the cathode surface to provide single electron calibrations. Light from a source such as a flashlight penetrated the thin aluminized mylar and ejected, via the photo-electric effect, a strong flux of individual electrons from the aluminum cathode. The actual photosensitivity of the cathode surface depended strongly on the previous history of the cathode surface. The single electron signal was also used on-line to calibrate discriminator levels directly in terms of number of electrons required to trigger the TDC discriminators.

The pulses observed from a test straw showed transitions from the proportional mode to saturated proportional mode to LS mode at critical voltages which were dependent on gas and pressure. Remarkably enough, with highly quenched gases that would normally be classified as being in the saturated proportional mode at 1 atm, with slow increases in Fe⁵⁵ gain as a function of voltage, we observed that at higher pressure the single electron induced pulses showed the discontinuous jump in gain characteristic of limited streamer operation. Beyond this transition the single electron induced pulses became nearly identical to those induced by the Fe⁵⁵ source. The pulses also had the characteristic very fast rise (~ 3 ns) and fall times associated with streamer formation.

Illustrative of this combined mode are typical results shown in Figure 9, showing the mean pulse height observed in these tests as a function of straw voltage. Note that although the single electron response increased by almost two orders of magnitude at the LS threshold, the Fe^{55} pulses were already saturated and did not change appreciably.

The characteristics of the LS mode at elevated pressure differed in another essential respect from limited streamers observed at lower pressures by other authors.^[11] Pulses associated with a Sr^{90} β source, which produces non-localized ionization, did not give predominantly single streamers, but rather gave large and variable pulses which could have up to ten times the amplitude and pulse duration of those produced by Fe^{55} . This can be explained by the Fe^{55} photon producing a tight cluster of ionization which produces a single streamer and a deadened region with a spatial extent of a few hundred microns. The lightly ionizing track, on the other hand, presumably produces a variable number of separate streamers, each with its own dead region. In spite of this variability, the sense wire supported counting rates in excess of 10^4 Hz/cm in the LS mode without appreciable dead-times.

The voltage plateau for these single electron streamers depended on the gas used. The plateau ended with the occurrence of characteristic regenerative breakdown pulses, separated in time by the electron drift time from anode to cathode. These clearly arose from UV photons, produced in the initial avalanche, causing photo-emission of electrons from the cathode. The cathode photo-sensitivity decreased and the gain plateau increased significantly with charge collected. (We could not distinguish whether this change was caused by surface cleanup or surface contamination). Typically, after "running-in" a straw, plateaus for single electron streamers were of the order of 800 V for heavily quenched gases at 4 atm.

Smaller wire diameters (20 – 40 μm) showed the combined property of long plateaus for both saturated proportional gain for large pulses and streamer behavior for single electrons. These wire diameters therefore provide an option of running in either mode. For this reason we chose to use 30 μm wires for use in the final chamber.

The use of LS pulses in drift time measurements has advantages aside from the obvious one of high gain ($\sim 10^7 - 10^8$.) These pulses are quite uniform, and have initial rise times shorter than a few nanoseconds, corresponding to electron collection rather than ion drift. In the saturated proportional mode, pulses from minimum ionizing particles have 50-100 times the amplitude of pulses from single electrons. Therefore in the LS mode the first electron produces almost the entire pulse height, as opposed to a small fraction, so that in the proportional region

cross-talk must be less than $\sim 1\%$ to trigger reliably on the first electron, while in LS mode thresholds can be raised, and crosstalk becomes unimportant.

5.2 CROSSTALK

In the following subsections, we present studies of position resolution which potentially can be realized if the problem of crosstalk between channels can be handled. The magnitude of the problem of course depends upon the particular electronic circuitry used.

In our test setup we measured crosstalk matrices for the entire system and its parts, using Fe^{55} photons. Elements in the system matrix ranged from 0.3% to 1.5%. The crosstalk was traced to incomplete shielding by the aluminum layer in the straw and to common grounding at the preamplifier output, in roughly equal parts. Some crosstalk pulses were inverted with respect to the primary pulse, while some were not. The pulses were highly differentiated and frequency dependent; slower rising pulses gave less crosstalk. Timing from crosstalk pulses is significantly slewed with respect to the primary pulses, because the crosstalk pulses are so small. Inverted crosstalk pulses were particularly delayed. We conclude that an upper limit on crosstalk of 0.5% is feasible.

5.3 RESOLUTION AND DRIFT VELOCITIES FOR VARIOUS GAS MIXES

Argon-Ethane, 50:50

Extensive measurements were made with the Argon-Ethane 50:50 gas mixture. Tests were made at 1, 2, 3 and 4 atm absolute pressure, with voltages spanning if possible the LS threshold, and at various discriminator settings. This gas has a drift velocity which is very nearly constant at the electric fields used.

It is instructive to present the results as scatter plots of arrival times on one straw versus another straw. Figure 10 displays such a plot for the staggered straw array showing the electron arrival time for straw 4, the offset straw, versus the arrival time for straw 1. If the drift velocity were exactly constant then the sum of the two times divided by the drift velocity would equal the offset between the two wires. The scatter plot shows a correlation very close to that expected for a constant drift velocity. Analysis of the small departures from linearity and use of the known straw offset permitted an accurate determination of the drift velocity as a function of position within the straw. The resolution as a function of position was also determined.

Figure 11 displays results from the 16 straw prototype with the sense wire plane tilted at an angle of 29° to the beam. This figure shows arrival times for

straw 1 versus straw 4 for operation at 4 atm. A cut was made to minimize backgrounds by demanding a very loose track fit of the hits in the other straws. Three regimes are apparent. Tracks crossing the array above or below both wire centers give rise to the parallel arms of linear correlation with the position within the straws. Tracks passing between the two wires give hits with a connecting negative correlation; the sum of the two time displacements is approximately constant for a saturated drift velocity. These three regimes are clearly seen in Figure 11. Additionally the behavior of tracks passing close to either of the wires can be seen from crossing times close to zero. A track going through the center of a sense wire can form its first cluster at a finite distance from the wire and so can result in a non-zero arrival time. This results in an observed time jitter of ~ 1 ns ($50\mu\text{m}$ in distance) in the vicinity of the wire. The observations are in agreement with predictions based on a detector threshold corresponding to the first electron arriving at the sense wire.

Use of the information from three straws permits correction for small effects from non-parallelism of the beam. To obtain resolution figures we used the following procedure. The passage of an 8 GeV/c particle through the drift cells was signalled by the occurrence of a scintillator pulse, which initiated the readout of TDC and ADC information. Tracks were selected by requiring either 4 TDC digitizations, or 3 TDC values in the case of determination of efficiency, which were fit to a straight line. Though the χ^2 cutoff was made very loose, in order not to cut off the tails of the distributions, no significant background remained.

For the data selected in this way, Figure 12 shows the distribution of the quantity

$$R = \sqrt{\frac{2}{3}} \left[\frac{t_1 + t_3}{2} - t_2 \right]$$

which can be shown to have a standard deviation equal to the single wire resolution. The distribution is well described by a Gaussian curve.

We have generally chosen to interpret the rms of the distribution as the position resolution, although it is generally larger than that obtained by fitting a Gaussian. To convert time to position resolution for Argon-Ethane, we have used a velocity of $50\mu\text{m}/\text{ns}$.^[12] The data of Figure 12 indicates an rms R of $20\mu\text{m}$.

Results of similar analyses at other pressures, voltages and discrimination levels are summarized in Figure 13. The highest voltage at each pressure above 1 atm was in the LS regime, where the resolution became essentially independent of the discriminator level. As voltage is reduced, R increases and becomes sensitive to discriminator setting. At 4 atm, resolution is excellent over a considerable range of voltages. At 1 atm, the resolution does not appear to reach a

limiting value in a way similar to that seen at higher pressure, and gets rapidly worse with decreased voltage.

The relative independence of resolution and discriminator level in the LS regime confirms the conclusions of the previous section that the first electron to drift to the wire controls the rising edge of the pulse. However, it should also be noted that at high pressures, resolution would not be degraded substantially if one were forced to run in the proportional mode, so long as the voltage remained near the LS threshold.

The dependence of resolution on distance from the wire is shown in Figure 14 at 4 atm for two voltages and two discrimination levels. The best overall result was for 4 kV, in the LS regime, where the effect of diffusion was barely visible. At 3.7 kV, in the proportional regime, resolution was only slightly worse but showed an expected deterioration near the wire, especially at high discriminator levels. The explanation is that electron collection proceeds substantially more slowly than for tracks away from the wire, causing the leading edge of the pulse to be more ragged. These results are compared to a solid and a broken line representing respectively which represent the result of a Monte Carlo simulation of the collection geometry.^[3] Agreement is good for a choice of diffusion constant $\sigma_d = 170\mu\text{m}\cdot\text{cm}^{-\frac{1}{2}}/\sqrt{P}$. This value agrees with our direct independent measurement of this quantity.

We have also explored the effect of tracks traversing the straws at an angle to the long axis of the straws. For operation at 4 atm we show resolution as a function of angle in Figure 15a. It is clear that the increase in effective ion density along the projected track path with angle gives improved resolution. Figure 15b shows the time resolution curve obtained at $\theta = 70^\circ$. It is double peaked because the fourth wire of the array had a $50\mu\text{m}$ offset with respect to the other three. This resolved the position ambiguity and made it possible to measure such small resolution.

Argon-Isobutane, 75:25

Argon-Isobutane mixtures are promising because heavy molecules are good quenchers. We tried a 75:25 mixture in conditions essentially identical to those used for the data of the previous section. The transition from proportional to LS modes occurred at roughly the same voltage as with the Argon-Ethane mixture. The results for resolution are so close to those of the previous mixture that we do not show them. We conclude that this mixture would be interchangeable with Argon-Ethane.

Argon-CO₂, 75:25

To obtain good lifetimes of the detector in a high radiation environment it

could be imperative to use mixtures without hydrocarbons. A possible choice is Argon-CO₂. We tried this in a 75:25 mixture at 2 and 4 atm.

This mixture does not have a saturated velocity characteristic, but does appear to have a high field plateau, although the actual values in the literature are inconsistent. We have used the values of Ma *et al.*,^[13] as given in the compilation of Ref. 12 and when converted for our straw geometry and 3300 volts, we find a velocity dependence on radius which is shown in Figure 16a. In Figure 16b we show our data for this voltage, with time converted to distance according to the velocity profile.

At 2750 volts, resolution had already deteriorated by ~ 50%.

5.4 DRIFT CHAMBER LIFETIMES

The main problem associated with the use of very high gains ($\sim 10^8$ for single electrons and associated average pulse gains of $\sim 10^7$) is chamber degradation. High gain coupled with an intense radiation environment must result in a large average DC current drawn by the chamber and eventual failure due to impurity layers deposited on either the cathode or the anode. We therefore made tests with a variety of gas mixtures. We expected, and have observed, that the use of flat cathodes permits the achievement of relatively long tube lifetimes.

Lifetime tests must be run at substantially higher rates than will be encountered with the actual apparatus, or they will require time greater than that for the ultimate use of the tubes. Our tests were made at 4 atm with a $10\mu\text{Ci Fe}^{55}$ source placed next to the straws. The applied high voltage was sufficient to produce limited streamer mode pulses at gains corresponding to ~ 150 mV into 50 ohms. The pulse rate was $\sim 30,000$ Hz corresponding to 1-2 μA per cm of wire.

The test straw was contained in a sealed pressurized vessel. The geometry and conditions differed in significant respects from previous tests,^[11,14] including the use of pressure, very high gains and a sealed gas volume.

Gases containing a large proportion of hydrocarbons such as ethane or isobutane went into continuous discharge mode after integrated currents of 0.05 C/cm. The discharge was caused by degradation of the anodes by the formation of "whiskers". If a new anode wire was inserted in the straw it would run for a similar period indicating that the problem was not connected with the cathode.

We therefore decided against quenching with organic gases and used CO₂ instead. Tests with Argon:CO₂ 50:50 allowed integrated currents up to 0.20 C/cm. At this point, disappearance of the aluminization on the cathode rendered the straw difficult to operate. We added 1% CH₄ in the hope that its positive ion

species would be less harmful to the cathode, and observed a slight improvement in lifetime to 0.25 C/cm. We settled on Argon:CO₂:CH₄ 49.5:49.5:1.0 as our operating mixture. [15] contains a more detailed account of our lifetime tests.

The use of Xenon as an additive^[16] was also tried. We have observed clean single electron streamer mode operation with a plateau of 900 volts and an ability to sustain currents in excess of 6 μA/cm in an Argon:Xenon:CO₂ 30:20:50 mixture at 4 atm pressure, without any added hydrocarbon quencher. In addition to the enhancement of avalanche multiplication by a large factor through the Penning effect Xenon appears to quench UV feedback, probably via its hard UV absorption bands centered at 1400 and 1200 AU.^[17] Straws operated with this gas mixture exhibited cathode damage after 0.25 C/cm integrated current.

5.5 CONCLUSIONS FROM PROTOTYPE TESTS

The results of resolution studies using the Argon-Ethane gas mixture showed good agreement with Monte Carlo predictions³ when values for the longitudinal diffusion constant of about $170\mu\text{m}\cdot\text{cm}^{-\frac{1}{2}}\cdot\text{atm}^{\frac{1}{2}}$ are used. The resolutions obtained under a wide variety of conditions for gases pressurized to 4 atm in a tube or straw configuration lie in the range 10-40 μm. At this level experimental precision is likely to be limited not by track resolution but by multiple scattering and other such constraints.^[18]

Straws can be operated at very high gains and can be used in a mode giving single electron limited streamers combined with strongly saturated Fe⁵⁵ pulses. This mode showed other qualitative differences from the limited streamers observed at lower gas pressures. The streamers appear to be confined to a region with spatial extent of only a few hundred microns and counting rates in excess of 10⁴ Hz/cm do not cause appreciable deadtimes.

Lifetimes for straw operation are good and similar to those observed for flat-cathode detectors used in other applications. The gas we have found to be best for lifetime is a mixture of Argon:CO₂:CH₄ in ratio 49.5:49.5:1 which gave a lifetime corresponding to an integrated charge on the anode of ~.25 C/cm. This mixture is reasonably well quenched, permitting operation at high gain with good chamber lifetime.

6. Vertex Chamber Performance.

6.1 ELECTRONICS

The Vertex Chamber electronics performed well, after some typical problems of grounding and noise were eliminated. Refer to Figure 5 for the layout of the Vertex Chamber and associated electronics. The electrical ground of the Vertex Chamber was insulated from the ground formed by the PEP beam pipe, to suppress pickup from the image currents of the beam itself. No pickup from this source was observed at the level of white noise from the preamplifiers. However, the long signal cables between the chamber and the preamplifiers proved susceptible to electromagnetic interference in the 1-100 MHz regime. Their susceptibility was reduced substantially by isolating both their center conductor and shield with 1-10 M Ω resistors from the high voltage supply cables. The dominant source of interference was the system for measuring drift times in the VC, the time to voltage converters (TVCs). Moving these from 10 meters to 30 meters from the preamplifiers reduced the total pickup to approximately the level of the white noise of the preamps.

The long cables limited the 10-90% rise time at their output to 4 ns, and attenuated signals from the chamber by 15%. The output slew rate of the preamps was 90 mV/ns, yielding a 10-90% rise time of 8.0 ns for pulses from Fe⁵⁵ sources in the chamber. The white noise of the preamps was 2.0 fC equivalent at their input with cables attached, 0.6 fC without. The low level of our discriminators was set at 6 fC input equivalent to the preamps, which corresponded to 30 mV at their output. Slewing and noise contributed less than .15 ns to our timing resolution.

TVC channels were calibrated with a CAMAC controlled delay generator. The delayed calibration pulse was injected at the preamplifier input, into half the channels at a time. For each channel, the delay time was fit as a quadratic function of the voltage output from the TVC. The non-linearity contributed only 0.5% to the calibration. This calibration was performed 8 times over the 17 months of data taking.

The channel by channel pedestals had a standard deviation of 15 ns; this was governed by the variability of a CMOS switch in the TVC circuit. Over the data taking period these pedestals were typically stable to 1.3 ns. The slope term in the quadratic fit was far more reproducible from channel to channel, varying only 1.3%; this was governed by one resistor and one charging capacitor. The drift was only 0.5% in these slopes.

The calibration reproduced input delays to better than 0.5 ns. During data taking, four spare channels were fed fixed delays; these indicated that the system

achieved a timing resolution over a typical two hour data taking run of 250 ps.

The combined effect of 1) slewing in the signal cables; 2) noise in the preamplifiers; and 3) resolution of the TVC system produces a timing resolution of < 300 ps. The maximum drift velocity in the Vertex Chamber was $100 \mu\text{m}/\text{ns}$. Therefore the degradation in spatial resolution from purely electronic sources was $< 30 \mu\text{m}$.

6.2 OPERATING POINT

The high voltage and threshold at which the chamber was operated was a compromise between spatial resolution and radiation damage considerations. As discussed in the introduction, for the short drift distances in our cells, triggering on the first arriving electron was desirable. At 3900 V, our threshold of 6 fC was very near the most probable signal for a single electron. Synchrotron X-rays were the dominant source of current drawn in the chamber. Approximately two random hits per beam crossing occurred in the chamber, causing a peak current of 3-5 nA/cm to be drawn in the innermost layer, at a high voltage of 3900 V. Higher voltages put the chamber in danger of accumulating more than 0.25 C/cm charge in the innermost layer over the life of the experiment, so we operated at 3900 V. In retrospect, we were slightly conservative; the innermost layer accumulated only 0.03 C/cm over the entire data taking period.

The two random hits per beam crossing interfered in no way with our track finding procedure. Electronic cross talk did not limit our ability to maintain a low threshold: studies with Bhabha events indicated that electronic cross talk produced $< 0.1\%$ of the hits in five of the six layers. However, knock-on electrons did produce hits in the cells immediately neighboring a cell penetrated by a track 1-2% of the time.

6.3 OFF-LINE CALIBRATIONS

We performed off-line calibrations of wire positions, drift timing constants, the time to distance relationship, and drifts in these quantities. Bhabha scattering events proved very useful for this purpose due to their simple topology, but their use is not in general mandatory. Multihadrons can be used if care is taken to avoid biases that occur in the regions dense with tracks.

Our calibration techniques require existing programs to link hits into tracks and to fit the track parameters. The programs used to do this are described in section 6.4 and [9].

Global Alignment

For a description of our tracking parameterization, see the Appendix. The VC measured only the three parameters that describe the track in the x-y plane. Of these three, only two were well measured, δ_{0vc} and ϕ_{0vc} . Systematic comparison of δ_{0vc} and ϕ_{0vc} with δ_{0cd} and ϕ_{0cd} as a function of ϕ_{0cd} , θ , and z_0 allowed determination of the five relevant parameters that describe the relative global orientation of the VC and the CD.

These five parameters were measured 13 times over the course of data taking. The horizontal and vertical translations were stable to 10 μm .

Time to Distance Calibration

The gas used in the Vertex Chamber, 49.5% Argon, 49.5%CO₂, 1%CH₄, has a drift velocity approximately proportional to the applied electric field. In a cylindrical geometry, this implies the drift distance r and the drift time t are related by $r \approx \sqrt{t}$. This simple relationship provided an initial guess for our time to distance function.

We improved the initial guess with the following procedure. Tracks in Bhabha scattering events with 4-6 hits in the VC and 7-10 hits in the CD were chosen. A VC hit was eliminated, and the remaining VC and CD hits were used in a new track fit. This new fit was used to predict the drift distance, r_{pred} , in the eliminated VC cell. Errors in the initial time to distance relationship tend to cancel in r_{pred} . We give a scatter plot of r_{pred} as a function of the measured drift time, t_{meas} in Figure 17. The $r_{pred} \propto \sqrt{t_{meas}}$ character is evident. We fit data such as that in Figure 17 to obtain the improved time to distance relationship, $r(t)$, or its inverse, $t(r)$. Fitting r_{pred} as a function of t_{meas} or vice versa yield systematically different results for short drift distances, because no drift distances are defined as negative. Furthermore, the large slope of \sqrt{t} near $t_{meas} = 0$ makes fitting r_{pred} as a function of t_{meas} difficult. Fitting t_{meas} as a function of r_{pred} proved to require fewer parameters and converged more easily. Cubic splines or orthogonal polynomials were used as fitting functions. The time to distance relationship converged to within 10 μm after one iteration of improvement. The relationship was evaluated five times over MAC data taking, usually after slight changes in gas mixture.

To account for drifts in timing, gas density, and electronics, run by run corrections were applied to the time to distance relationship. A typical run lasted 90 minutes and yielded 100 Bhabha scattering events for calibration. The drift time actually used in the time to distance relationship, t , was computed from

$$t = t_{0rr} + s_{rr} \times t_{meas}$$

where t_{0rr} and s_{rr} are the run by run timing offset and slope. These are found using a procedure very similar to that used to extract the time to distance relationship. Typically t_{0rr} could be measured to an accuracy of .2 ns and s_{rr} to 2%. t_{0rr} remained stable for weeks, then would suddenly shift, usually due to a power failure or changes in PEP timing. The slope term was very stable, reflecting the stability of the gas density.

Channel by Channel Calibration

The timing constants and physical positions of each cell were calibrated offline. The procedure was similar to that used to obtain the time to distance calibration. The residuals $\delta r = r_{pred} - r(t_{meas})$ and $\delta t = t(r_{pred}) - t_{meas}$ were fit for each cell with four constants:

1. An offset in time, t_0 .
2. An offset in distance, in the azimuthal direction, d_0 .
3. A slope in time, s .
4. A tilt in z , the axial direction.

d_0 and t_0 effect δr with opposite signs on opposite sides of the sense wire. In a typical calibration, 100 runs were used, corresponding to 6 pb^{-1} of integrated luminosity. This yielded approximately 150 residuals in each of the 324 cells. The largest correction was d_0 . The standard deviations of d_0 for each cell over the 13 measurements also indicated a reproducibility and/or stability of $10 \mu\text{m}$.

The channel by channel calibrations were made in a single pass through Bhabha scattering data. The improvement in spatial resolution due to the calibration was then immediately known via the multivariate analog of the relationship:

$$\sum_{i=1}^N (x_i - \bar{x})^2 = \sum_{i=1}^N x_i^2 - N\bar{x}^2$$

Use of orthogonal polynomials as fitting functions allowed straightforward isolation of the contribution of the various constants. Table 2 gives the importance of each of the constants.

The miscalibration of a single channel in the Vertex Chamber 'pulls' the track fit and therefore can induce an apparent miscalibration of channels in other layers. This coupling was not explicitly accounted for in our calibration procedure. The offsets in azimuth between layers tend to reduce the importance of this effect. Further, when performed multiple iterations of the calibration procedure we found the constants after one iteration were within $10 \mu\text{m}$ of their values after three iterations.

Certain correlations between distant cells were found to occur. For example, the initial channel by channel calibration resulted in a slight uniform translation of all cells by an equal distance in the azimuthal direction. This created the appearance that the tracks in Bhabha scattering events were tangent to a circle centered on the geometric center of the chamber. The effect was eliminated by constraining the two tracks in a Bhabha event to have equal but opposite distances of closest approach to the geometric center of the chamber. This constraint was made only for the track fits used to determine the calibration constants. Similar distortions in the mean acollinearity and momentum difference were observed and suppressed. In general, correlations between distant cells are not necessarily well constrained in our cell by cell calibration procedure. However, spurious correlations are easily removed by constrained fitting of tracks, or by constraint of the final survey constants.

6.4 PATTERN RECOGNITION

Algorithm

Track segments were obtained by independent pattern recognition programs in the CD and the VC. The CD algorithm took account of the full three-dimensional helical form of the trajectory, detected with information from the stereo layers. This algorithm is described in [9]. The VC algorithm was simpler, because tracks are approximately straight lines in the VC.

We regard the six layers of the VC as three double layers for the first step of pattern recognition. Because of the overlapping, regular geometry of the VC double layers, the drift distances r_1 and r_2 for hits produced by a radial track are related by:

$$r_1 + \frac{R_1}{R_2} r_2 \approx r_0 \quad (6.1)$$

Here R_1 is the radius of layer 1 or the double layer, R_2 that of layer 2, and r_0 the straw radius. Pairs of hits in double layers were associated if they met (6.1) within $200 \mu\text{m}$. Random associations were thereby suppressed, with little loss of real tracks. Most loss of real tracks occurred for very low momentum tracks or tracks from very long lived species, such as K^0 s and Λ s. The ambiguity of which side of the sense wire the track passed is resolved by (6.1) in most cases.

Associated pairs in the three double layers were then linked based on their agreement in azimuth. A straight line fit was made to the resulting set of hits and drift distances. The straight lines found in the VC were then compared to and matched with tracks found in the CD. Unmatched CD tracks were extrapolated into the VC and a search made for VC hits. A weighted, least squares fit

was performed to both the VC and CD hits and drift distances. VC hits were assigned weights based on the measured resolution as a function of drift distance (Figure 17). Multiple scattering was accounted for by allowing partially constrained kinks at the beam pipe, the boundary between the VC and CD, and at fixed locations within the chambers. A final search was made for hits along the track fit, and .1% of the VC and CD hits were dropped due to large residuals.

Efficiency

The efficiency of the VC was measured by using a sample of tracks well measured in the CD. Sources of inefficiency include dead cells, overlap of particle trajectories, and inadequacy of the track finding algorithm for particles with low momentum or very large impact parameter.

Well measured tracks in the CD by four requirements: 1) ten hits from the CD must be linked to the track, 2) $z_{0cd} \leq 5$ cm., 3) $\theta \leq 20^\circ$, and 4) $\hat{\chi} \equiv \sqrt{2\chi^2 - \sqrt{2n_D - 1}} \leq 4$. Table 3 gives the efficiency for well measured CD tracks to link to ≥ 3 VC hits. The Bhabha efficiency was determined from 2 pb^{-1} of integrated luminosity, tau lepton and multihadron efficiencies from 94 pb^{-1} .

Track overlap was a source of inefficiency in the VC in multihadron events. If two tracks were separated by less than the diameter of a straw, 6.9 mm, they could leave only one hit in a layer of the VC. The staggering of VC layers usually prevented this phenomenon from happening in every layer. Double-hit electronics probably could not eliminate it, because the drift field for straws is radial. Figure 18 shows the efficiency for well measured CD tracks to link to ≥ 3 VC hits as a function of VC track separation. The VC track separation is the minimum distance in the azimuthal direction from the well measured track to the nearest CD track, within the VC boundary. The efficiency was near 50% for small separation, indicating one track of the overlapping pair was found in the VC. For large separations, the efficiency was better than 96%.

The VC track finding algorithm was most efficient for straight tracks coming from the beam centroid. The efficiency for CD tracks with VC track separation greater than one straw diameter was studied as a function of momentum and impact parameter. The efficiency was $\geq 90\%$ above $200 \text{ MeV}/c$. Tracks softer than $500 \text{ MeV}/c$ had an error in impact parameter due to multiple scattering in the beam pipe equal to their error due to chamber resolution. Since the multiple scattering error scales as $1/p$, tracks with $p < 200 \text{ MeV}/c$ contribute little information to lifetime measurements. The efficiency versus impact parameter was flat from 0. to beyond 3 mm. Typical impact parameters of particles from B -meson decay are $300 \mu\text{m}$, so we conclude that linking efficiency effects lifetime measurements very little.

Well measured tracks in the VC can be used to measure the efficiency of the CD. Defining a well measured track as one with six hits in the VC, 0.932 ± 0.001 are matched with tracks having six or more hits in the CD, and 0.798 ± 0.001 are matched to tracks having seven hits or more.

6.5 OBSERVED RESOLUTIONS

Spatial resolutions were measured with residuals from the track fit. If the VC hit used to measure the residual is left in the track fit, the resulting residual distribution is systematically narrower than the true residual distribution, due to the pull of the hit in the fit.^[19] Conversely, if the hit is removed from the fit the distribution is wider than the true distribution, due to interpolation error in the track fit. The size of the bias is almost equal in these two cases, but opposite in sign. Figure 19 displays the residuals from Bhabha scattering events, where VC hits were removed from the fit. The non-gaussian tails arise from the variation of resolution with drift distance. The resolution as a function of drift distance is shown in Figure 20. Over most drift distances, the resolution is $35 \mu\text{m}$. Near the wire the resolution degrades, most probably due to the dispersion in pulse heights in our gas mixture, which is underquenched. Estimates of degradation due to spacing of ionization clusters, and due to timing resolution, indicate that these do not provide the degradation of resolution near the wire. The mean resolution is $45 \mu\text{m}$.

The figure of merit for lifetime measurements is σ_v , the resolution in extrapolated distance of closest approach to the geometric center of the chamber. σ_v depends on the position resolutions of both the VC and the CD, the radii of their sense wires, and the amount of matter that causes multiple scattering in the beam pipe:

$$\sigma_v^2 \approx \frac{\bar{\sigma}^2}{N} (1 + f_1^2(\bar{\rho}) + f_2^2(\bar{\rho})) + \frac{\sigma_p^2}{p^2} \quad (6.2)$$

The first term arises from the non-zero measurement resolution in the drift chambers, the second from multiple coulomb scattering. Here $f_1(x)$ and $f_2(x)$ represent the errors in extrapolation due to the slope and curvature in the fit, and are polynomials of order 1 and 2 respectively:

$$f_1(x) = x$$

$$f_2(x) = \frac{x^2 + \gamma_{1r}x + 1}{\gamma_{2r} + \gamma_{1r}^2 + 2}$$

$\bar{\rho}$, the dimensionless mean extrapolation distance, is $\bar{\rho} \equiv \bar{r}/\sigma_r$; given the radii

$\{r_1, \dots, r_N\}$ of the sensing layers, and their spatial resolutions $\{\sigma_1, \dots, \sigma_N\}$,

$$\bar{r} \equiv \frac{\bar{\sigma}^2}{N} \sum_{i=1}^N \frac{r_i}{\sigma_i^2} \quad , \quad \frac{1}{\bar{\sigma}^2} \equiv \frac{1}{N} \sum_{i=1}^N \frac{1}{\sigma_i^2} \quad , \quad \sigma_r^2 \equiv \frac{\bar{\sigma}^2}{N} \sum_{i=1}^N \frac{1}{\sigma_i^2} (r_i - \bar{r})^2 \quad ,$$

and γ_{1r} and γ_{2r} are the coefficients of skew and curtosis defined in analogy with σ_r . For the combination of CD and VC, $\bar{r} = 8.6$ cm, $\sigma_r = 7.4$ cm, $\gamma_{1r} = 3.5$, and $\gamma_{2r} = 15$. $f_1^2(\bar{\rho}) = 1.4$, while $f_2^2(\bar{\rho}) = 12$, indicating that uncertainty in the curvature in the fit dominates the extrapolation error. This uncertainty arises primarily from the small maximum radius, 45 cm, of the MAC CD; the vertex resolution decreases as the *square* of this radius. The first term in (6.2) predicts a vertex resolution of $72 \mu\text{m}$ for $45 \mu\text{m}$ resolution in the VC. In the second term σ_p depends on the angle of the track with respect to the beam axis, but was typically $65 \mu\text{m-GeV}/c$.

The resolution in impact parameter was measured with Bhabha scattering events. Ideally, the opposing electron tracks would have equal and opposite impact parameters. Figure 21 shows the sum of the measured impact parameters. The distribution is very gaussian, with fitted σ of $124 \mu\text{m}$. This indicates a resolution $\sigma_v = 124/\sqrt{2} = 87 \mu\text{m}$ in impact parameter. Constraint of the momentum leads to $\sigma_v = 52 \mu\text{m}$.

The effective spatial resolution in the VC was $\approx 70 \mu\text{m}$ in multihadron events. The primary source of this degradation was the misassociation of hits with tracks in the dense environment of a multihadron event. Hits in adjacent cells due to knock-on electrons probably caused some confusion as well.

The resolution in extrapolated distance of closest approach, or impact parameter, in multihadron events is given in Figure 22. Tracks with: 1) 3 or more hits in the VC; 2) 7 or more hits in the CD; and 3) momenta $> 500 \text{MeV}/c$ were used. The first plot makes use of the beam centroid, as determined from Bhabha scattering events on a run-by-run basis. The resolution in this case is dominated by the size of the beam itself, which we measured to have $\sigma_x = 350 \mu\text{m}$ and $\sigma_y = 70 \mu\text{m}$. For the second plot, an improved estimate of the e^+e^- annihilation location, the ‘average vertex,’ was made on an event by event basis. These data indicate a vertex resolution of $210 \mu\text{m}$, of which $110 \mu\text{m}$ was due to multiple coulomb scattering.

Finally, we show in Figure 23 the VC hits observed and the tracks fitted to them, for an event interpreted as coming from τ -lepton pair production, with each τ decaying into three charged particles. The hits are represented by circles, to which the track associated with them should be tangent. It should be noted that the figure is quite representative of the low number of accidental hits observed.

7. Overall Conclusions

We have described the design and construction of a Vertex Chamber using a coaxial tube geometry, colloquially known as a straw chamber. We have justified the choice of this technique, in a way intended to help other experimenters decide the most appropriate choice for them. Briefly, we chose this design for its ruggedness, its ease and speed of construction, its ability to obtain high spatial resolutions, its cell size and hence low occupancy allowing use of single hit electronics, and its potential for long life in an environment with high radiation levels. These characteristics are not specific to our experiment, but are required by other detectors in colliding beam experiments, such as those projected for future high luminosity hadron colliders.

We have described the procedure used to design the shielding needed to place a chamber at about 3 cm from the PEP beam line. The resulting configuration resulted in extremely quiet operation of the VC.

We have also given the results of tests with a chamber prototype used in a test beam to study the spatial resolution as a function of electric field, pressure, and gas mixture. The resolution improves dramatically with pressure both because intercluster distance decreases and because diffusion is decreased. Increased pressure also allows more stable operation in the limited streamer mode, where a single electron can generate a pulse which rises as fast as, and is as big as, one from a large ionization cluster. However in this mode average currents are much larger than for the proportional mode, leading possibly to rapid chamber deterioration.

Lifetime studies of a variety of gases were presented. The best lifetime, along with LS response, was obtained with a gas mixture of Argon:CO₂:CH₄ in the ratios 49.5:49.5:1. The lifetime was $\sim .25$ C/cm.

Finally the performance of the Vertex Chamber in operation was discussed. Our calibrations and pattern recognition algorithm were described. These were used to estimate the effective position resolution of the device, which was $45\mu\text{m}$, and the vertex impact parameter resolution, which was $87\mu\text{m}$.

We conclude that the technique of constructing a chamber with straws has completely fulfilled the requirements of our experiment, and that the characteristics of such a chamber permit a wide range of tracking applications in high radiation environments.

APPENDIX

Five parameters describe the helical trajectory of charged particles in the axial magnetic field of MAC. Three of these describe the circular projection of the trajectory in the plane perpendicular to the beam axis: κ , the reciprocal of the radius of curvature; δ_0 the (signed) distance of closest approach of the circle to the geometric center of the MAC coordinate system; and ϕ_0 , the azimuth of the trajectory at closest approach. The sign of δ_0 is determined from the cross product of the direction of the particle trajectory at closest approach taken with the direction from the geometric center to the point of closest approach. Figure 24 exhibits the definition of κ , δ_0 , and ϕ_0 . The remaining two parameters describe the particle trajectory out of the plane perpendicular to the beam. θ is the angle with respect to the beam axis of the trajectory, and z_0 its intercept with the axis, viewed along the azimuth containing the distance of closest approach.

In the MAC track fitting routines, multiple coulomb scattering is described by 'kinks' at the radii of matter concentrations, such as the boundary between the VC and CD. Several kink angles are fit, but with a constraint by the r.m.s. angle predicted by multiple coulomb scattering. This procedure quite naturally incorporates errors from multiple coulomb scattering into the covariance matrix of κ , δ_0 , ϕ_0 , θ , and z_0 .

ACKNOWLEDGEMENTS

We gratefully acknowledge discussions we have had with E. Iarocci, D. Rust, and J. Jaros. We also wish to thank E. Askeland, J. Broeder, N. Erickson, and J. Escalera, for their superb technical work. We would especially like to acknowledge and remember the late T. Pulliam, the engineer responsible for installation of the Vertex Chamber in MAC. We gratefully acknowledge the help of the PEP and MAC Operations groups and in particular N. Palmer and D. Wright in the Vacuum Group of the Klystrons Task Force. Finally R. Gearhart's help with the test beam setup is appreciated.

REFERENCES

- (a) Present address: MPI, Munich, FRG
- (b) Present address: CERN, Geneva, Switzerland.
- (c) Present address: Laboratorio de Fisica de Altas Energias, Universitat Autònoma de Barcelona, Barcelona, Spain.
- (d) Present address: Texas Accelerator Center, The Woodlands, TX 77380.
- (e) Permanent address: Physics Department, University of Padua, Padua, Italy.
- (f) Present address: University of Oslo, N-0316, Olso 3, Norway.
- (g) Present address: Enrico Fermi Institute, University of Chicago, Chicago, IL 60637.
- (h) Joint appointment: Department of Physics and College of Computer Science, Northeastern University, Boston, MA 02115.
 - 1. G. Charpak *et al.*, Nucl. Instrum. and Methods **99**,279(1972).
 - 2. D. Rust, SLAC-PUB-3311, April 1984.
 - 3. G. Chadwick and F. Muller, MAC Internal Memo No. 683, Feb. 1984.
 - 4. J. Va'Vra, SLAC-PUB 3131, June 1983.
 - 5. J. A. Jaros, Stanford 1982: Proceedings, Instrumentation for Colliding Beam Physics (1982); SLC Workshop Note No. 51, Dec. 1981
 - 6. A. Boyarsky, SLC Workshop Note No. 2, Feb. 1983.
 - 7. C. T. Hoard, SLAC-TN-82-3, October 1982.
 - 8. Precision Paper Tube Company, 1033 So. Noel Street, Wheeling, Illinois, 60090 USA.
 - 9. E. Fernandez *et al.*, SLAC-PUB 4048 (in preparation), and to be published.
 - 10. C. Logg and P.W. Clancey, SLAC Electronics Dept. ELDDOC No.25, 1983.
 - 11. E. Iarocci, Nucl. Instrum. and Methods **217**, 30 (1983); M. Atac and A. V. Tollestrup, Preprint FN-339, Fermilab (1981); T. A. Mulera and V. Perez-Mendez, Nucl. Instrum. and Methods **203**, 609 (1982); T. A. Mulera *et al.*, IEEE Trans. Nucl. Sci., NS-**30**, 355 (1983).
 - 12. see, *e.g.*, J. Fehlmann *et al.*, Compilation of Data for Drift Chamber Operation, ETH ZURICH, HPK, TEC DETECTOR GROUP, July 1982. We have also measured this quantity directly.

13. C. M. Ma *et al.*, MIT Technical Report 129 (1982).
14. A. H. Walenta, Proceedings of the 1977 Isabelle Summer Workshop, p. 41, (1977); Results of Fischer, Sobottka and Walenta, quoted by H. Okuno *et al.* in Proceedings of the 1978 Isabelle Summer Workshop, p. 139 (1978); H. J. Hilke, Proceedings of the 1981 Isabelle Summer Workshop, p. 1275 (1981).
15. H.N. Nelson "Lifetime Tests for MAC Vertex Chamber," SLAC-PUB-4017, in *Workshop on Radiation Damage in Wire Chambers, Berkeley, CA*, edited by J. Kadyk (Lawrence Berkeley Laboratory, Berkeley, CA, 1986).
16. R. Z. Fuzesy *et al.*, Nucl. Instrum. and Methods **100**, 2567 (1972).
17. G. Baldini, Phys. Rev. **128**, 1562 (1962).
18. G. Chadwick, MAC Internal Memo No. 688, Feb. 1984.
19. F. Solmitz, Ann. Rev. Nucl. Sci. **14** 375 (1964).

TABLE CAPTIONS

1. Matter in the Vertex Chamber Assembly.
2. Contributions of Survey Terms. These are the contributions to the *uncorrected* spatial resolution that may be attributed to the various survey corrections. The tilt in z indicates a deviation of the ends of the sense wires from their average position of $38 \mu\text{m}$.
3. Vertex Chamber Efficiency.

Inner Radius	Thickness		Material	Name
	cm	X_0 , %		
3.564	0.0075	0.21	Titanium	X-ray Absorber
3.571	0.1118	0.32	Beryllium	Beam Pipe
3.683	0.0050	0.02	Kapton	Electrical Insulator
3.843	0.0762	0.22	Beryllium	VC Spool Column
4.582-8.405	-	0.76	Mylar, Tungsten, Argon, CO ₂ , CH ₄	Straws, Wires, Gas
9.024	0.0064	0.02	Mylar	Electrical Insulator
9.035	0.254	2.85	Aluminum	Pressure Vessel Wall

Table 1

Correction	Contribution (μm)
t_0	48
d_0	49
s	20
tilt in z	11

Table 2

Events	VC Efficiency
Bhabhas	0.994 ± 0.001
Taus	0.982 ± 0.003
Multihadrons	0.939 ± 0.001

Table 3

FIGURE CAPTIONS

1. Cross section of the MAC Vertex Chamber, shielding and beam pipe assembly. The close-in collimators, or 'Tantalum Scrapers' are shown. Also shown are the heavimet shielding that is intended to absorb the showers initiated by overfocussed electrons, the titanium liner designed to absorb fluorescence from the Tantalum Scrapers, and the BGO.
2. Layout of the Vertex Chamber endplate, showing the arrangement of the 6 layers of tubes.
3. Detail of the end fitting for straw and wire. See the text for a discussion of most elements. The washer was waved to act as a spring, allowing uniform tension to be applied to the straws.
4. Photograph of the Vertex Chamber under construction. The white tips of the Delrin plugs and the metal feedthroughs are visible.
5. Electronic Layout of the Vertex Chamber. Straws are terminated in approximately their characteristic impedance at one end; signals go from the straw's other end, through 19 meters of coaxial cables to the preamplifiers, then to the discriminators and finally the TVC (time to voltage) drift time measuring system.
6. LABEN 5242 Preamplifier. The input integration stage, pole zero network, and output buffers are shown. The $5.3 \text{ k}\Omega$ feedback resistor was added to narrow the bandwidth, which lead to reduced sensitivity to electromagnetic interference.
7. Photograph of the prototype.
8. Schematic of the electrical circuit used in the prototype tests of the MAC Vertex Chamber.
9. Mean pulse height as function of voltage in Argon-Ethane at 4 atm. The straw diameter was 6.9 mm, the wire diameter $20 \mu\text{m}$.
10. Drift times for two straws offset with respect to the beam by one radius, plotted one versus the other. For constant velocity, their sum is constant.
11. Drift times for two straws tilted at an angle of 29° to the beam, plotted one versus the other. The region of constant sum for the times is smaller and two regions of constant difference emerge.
12. Distribution of the resolution quantity R , for Argon-Ethane 50:50 at 4 atm, $V=4.15 \text{ kV}$. The curve is a Gaussian distribution fitted to the data, with $\sigma = 0.4\text{ns}$, corresponding to $20\mu\text{m}$ resolution.

13. Average single wire resolution as a function of voltage scaled by pressure for various pressures and discriminator levels. The curves are to guide the eye only.
14. Dependence of resolution on distance from the wire, for Argon-Ethane 50:50 mixture at 4 atm. The solid circles are for 4 kV at which pulses are in the LS regime. Open circles and crosses are for 3.7 kV, proportional mode. Here resolution is not markedly worse, but the region near the wire shows deterioration, especially at higher discrimination level. The solid line is the result of a computer simulation study of pulse formation by ionization in straws.
15. a) Single wire resolution of the straws as a function of the angle θ from normal incidence. The increase of effective ion density with angle appears to give considerable improvement. b) Time resolution curve for the 70° data. The curve is a fit to a double Gaussian distribution with one variance, used in obtaining the resolutions quoted. The separation results from a $50\mu\text{m}$ offset of the fourth wire.
16. a) Velocity profile of a mixture of Argon-CO₂ in 75:25 ratio used in the straw electric field configuration. b) Resolution found as function of track distance from the wire.
17. Time to Distance Relationship. The drift time is that measured in a cell of the VC, t_{meas} . The drift distance is obtained by dropping that cell from the track fit, then predicting the drift distance in the missing cell. In this manner the cell's 'pull' in the track fit is avoided. A fit is made to data like that above to obtain the functional time to distance relationship.
18. Effect of Track Overlap on VC Efficiency.
19. VC Residuals. The hit was *removed* from the track fit in these data. Residuals for all drift distances are in (a), where the fitted gaussian has $\sigma = 45\mu\text{m}$. In (b), only data from distances $> 0.15\text{ cm}$; the fitted gaussian has $\sigma = 38\mu\text{m}$. As discussed in the text, these data *overestimate* the spatial resolution of the chamber.
20. VC Spatial Resolution. The fitted σ of the residual distribution is shown as a function of drift distance. Both cases of hit left in the track fit and removed are shown. The true σ is approximately half way between these two extremes.
21. 'Miss' distance in Bhabha Scattering Events. These data show the sum of the δ_0 s for the two tracks in Bhabha events. In (a), the momenta were allowed to vary in the track fit. The distribution is very gaussian, with $\sigma = 124\mu\text{m}$. In (b), the track momenta were constrained to beam energy,

and the distribution narrowed to $\sigma = 74 \mu\text{m}$. This indicates the importance of the term arising from track *curvature* in (6.2).

22. Vertex Resolution in Multihadron Events. These data show the distance of closest approach of tracks with respect to two estimates of the e^+e^- annihilation point. In (a), the estimate is the beam centroid, as determined in Bhabha scattering events. The fit is to a Student's t distribution, with $\sigma = 306 \mu\text{m}$ and asymptotic power 1.9 describing the tails. In (b), the 'average vertex' was used; the fit yields $\sigma = 210 \mu\text{m}$ and power 1.5. (c) and (d) are the same as (a) and (b), except plotted on a logarithmic scale to exhibit the tails.
23. Hits in the VC from a τ -lepton pair production event in MAC. The hits are represented by circles corresponding to the measured drift distances, and tracks are fitted to be tangent to these circles.
24. Parameters Describing a Particle Trajectory. The figure is in the plane perpendicular to the beam. The outer circle schematically represents a boundary in the drift chamber system. δ_0 is given a sign based upon the cross product of a vector pointing along the particle trajectory taken with a vector from the geometric center to the perihelion of the trajectory. The trajectory shown has $\delta_0 > 0$ but $\kappa < 0$ in our convention.

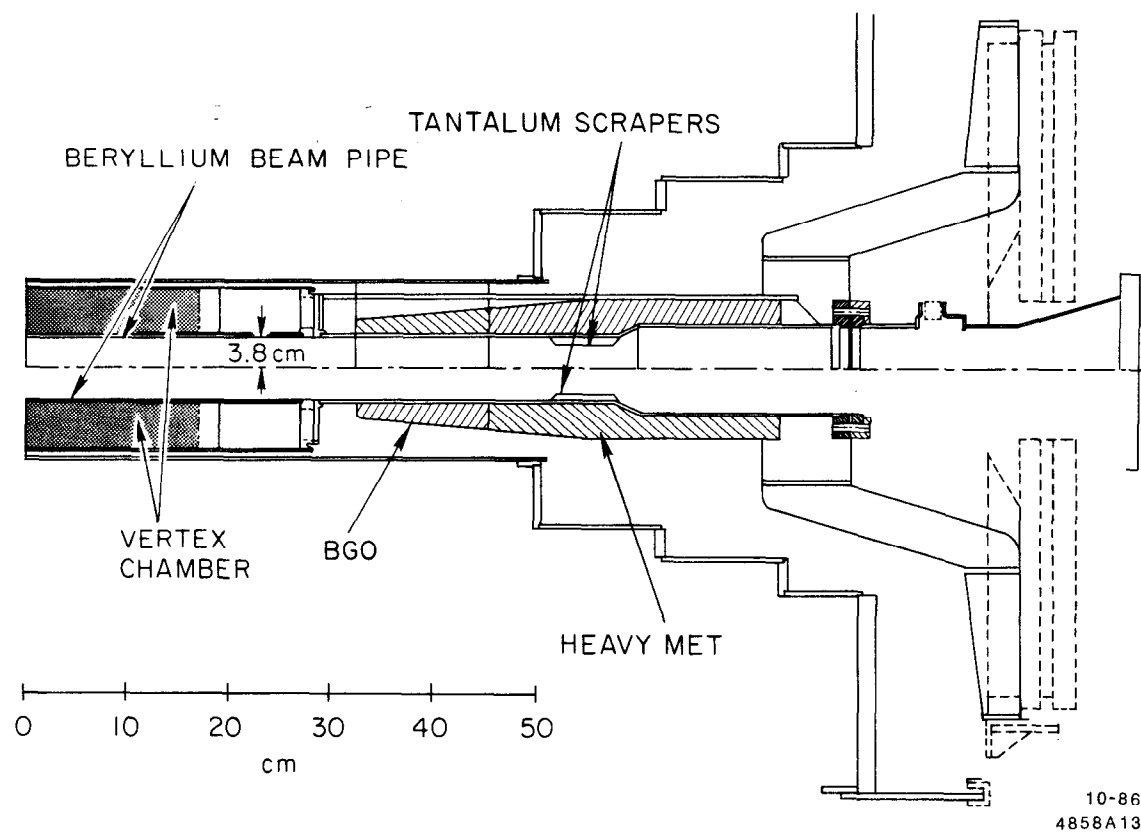
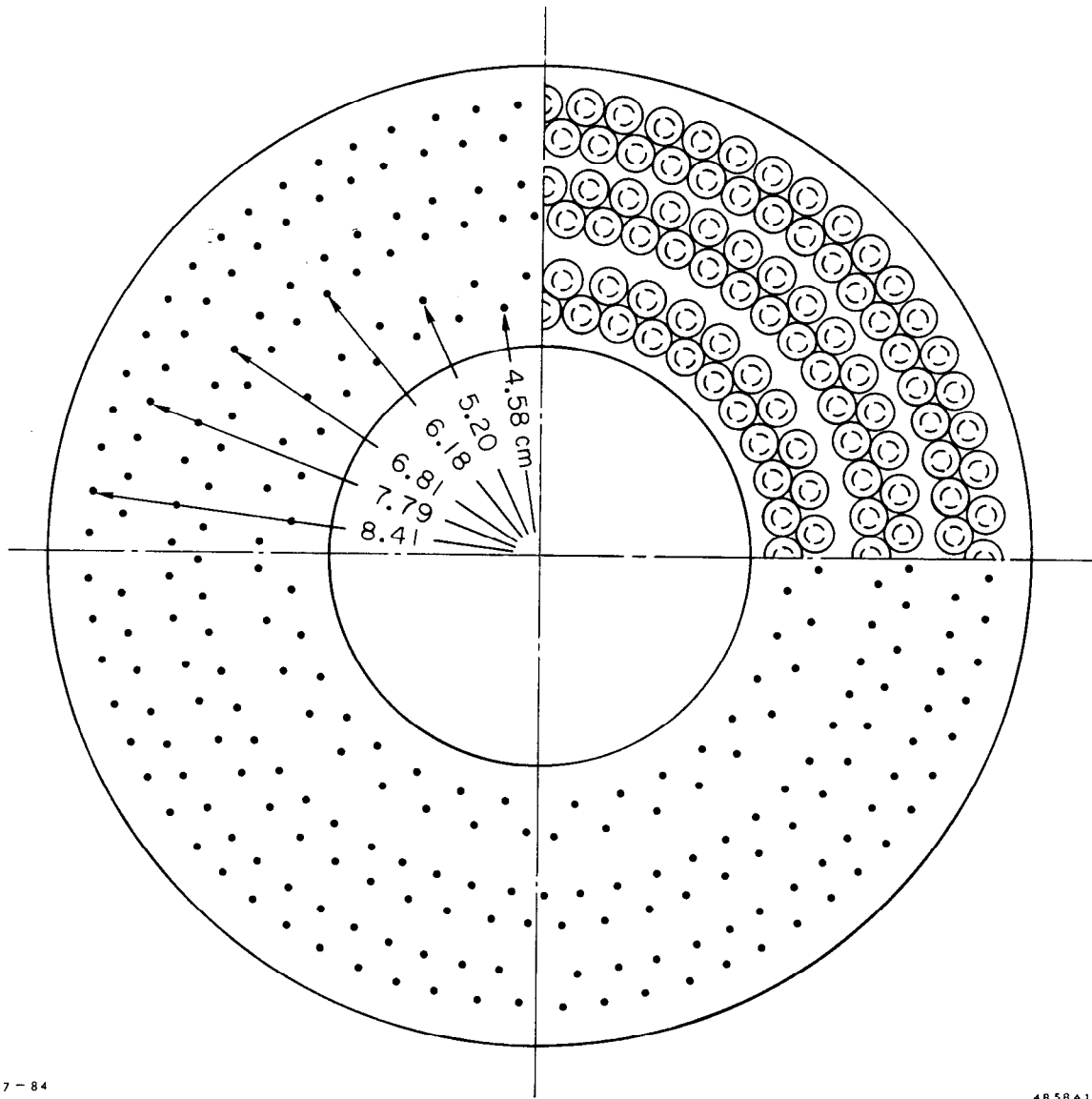


Fig. 1



7-84

4858A1

Fig. 2

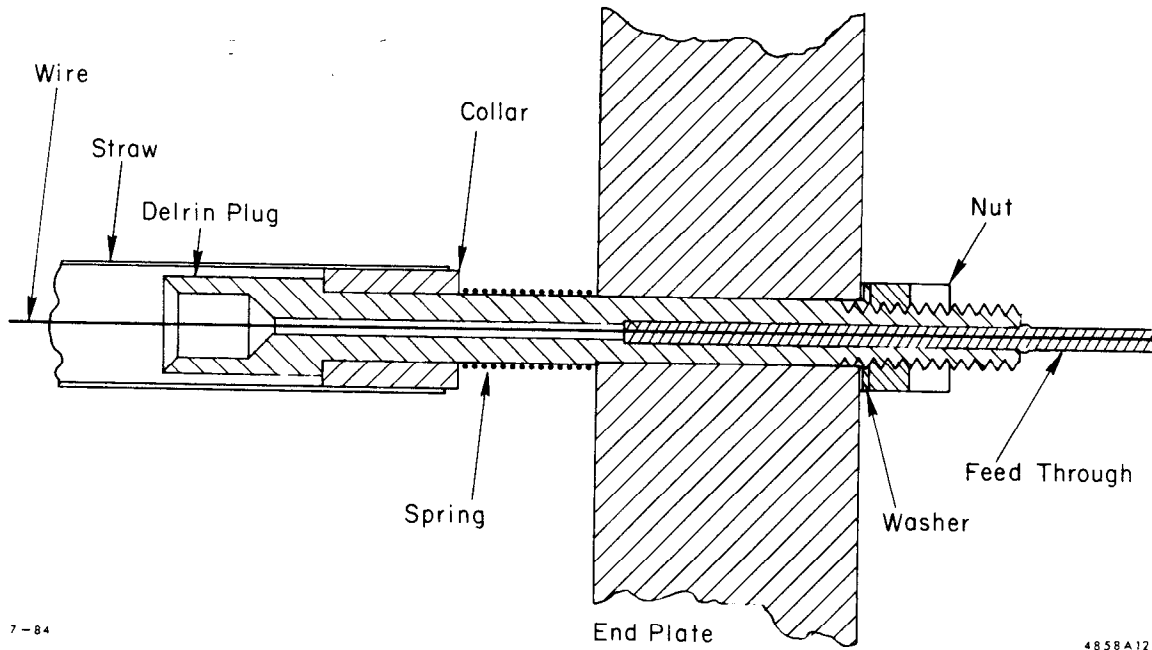
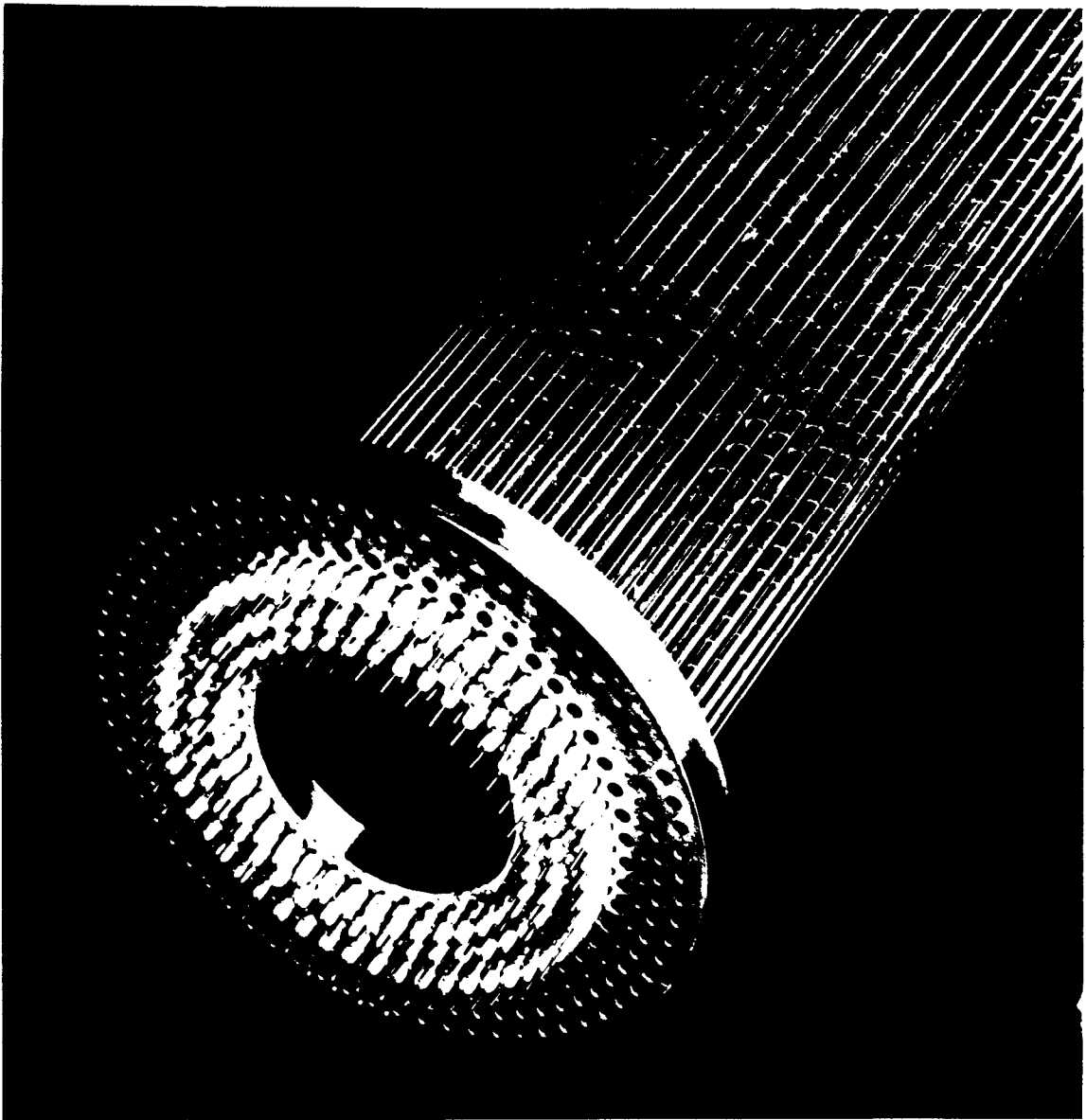


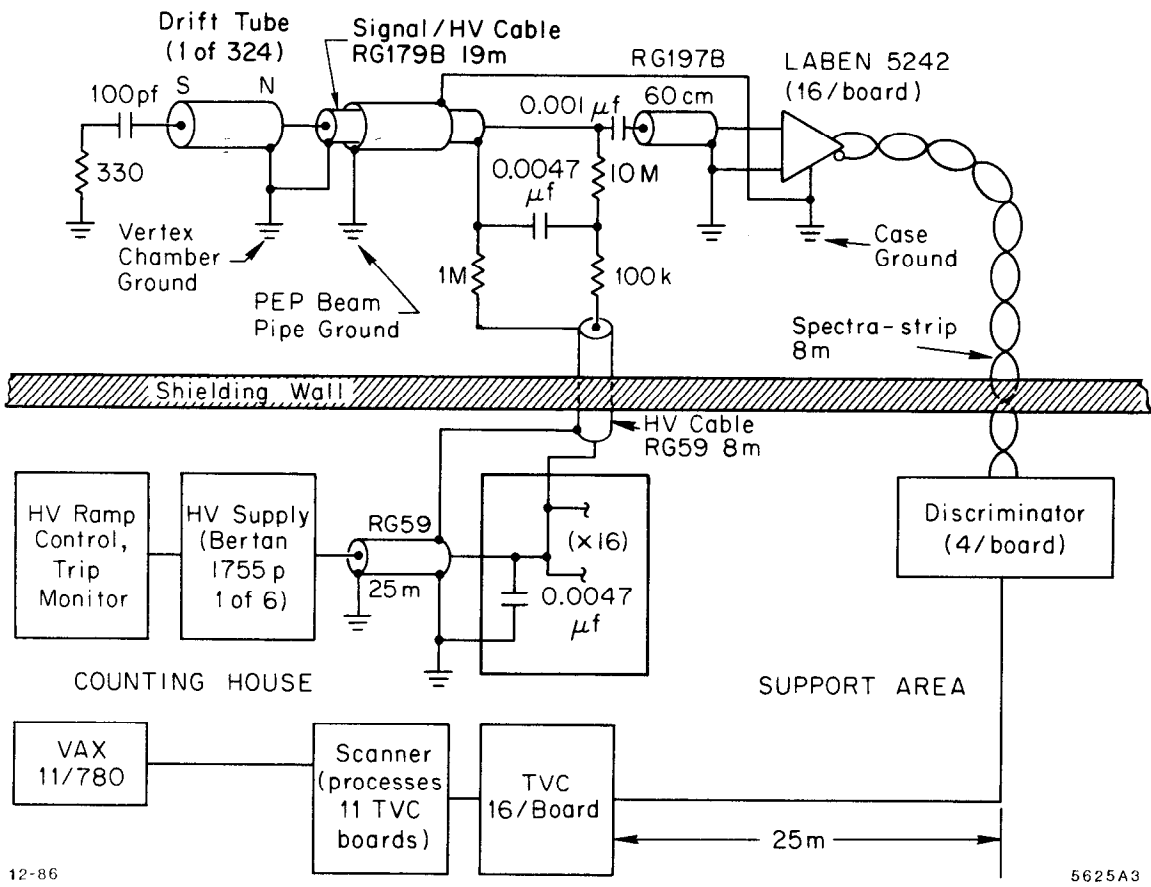
Fig. 3



8-84

4858A14

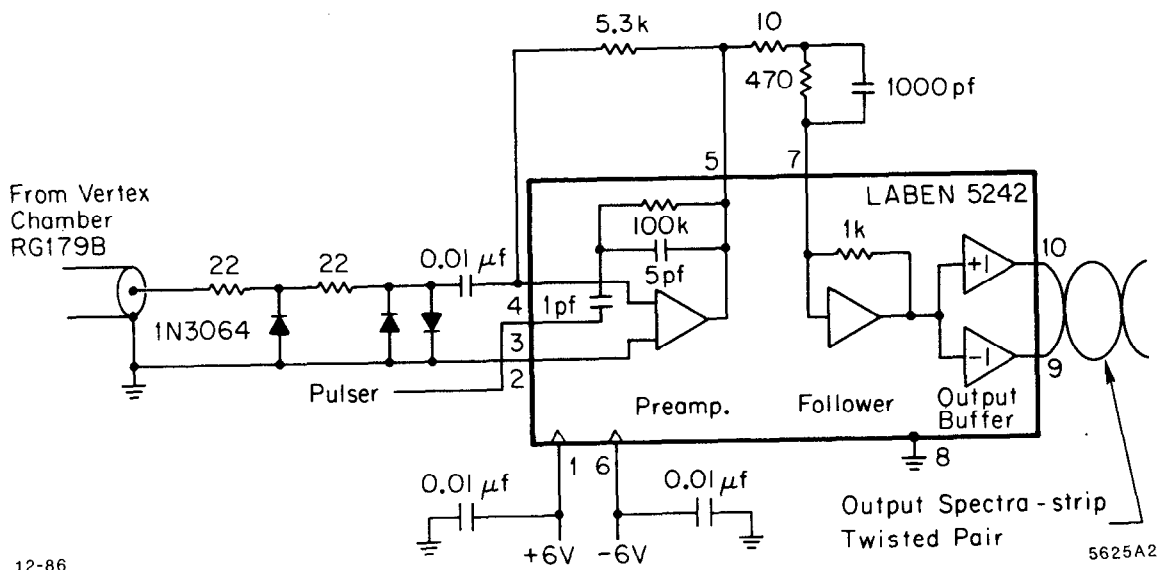
Fig. 4



12-86

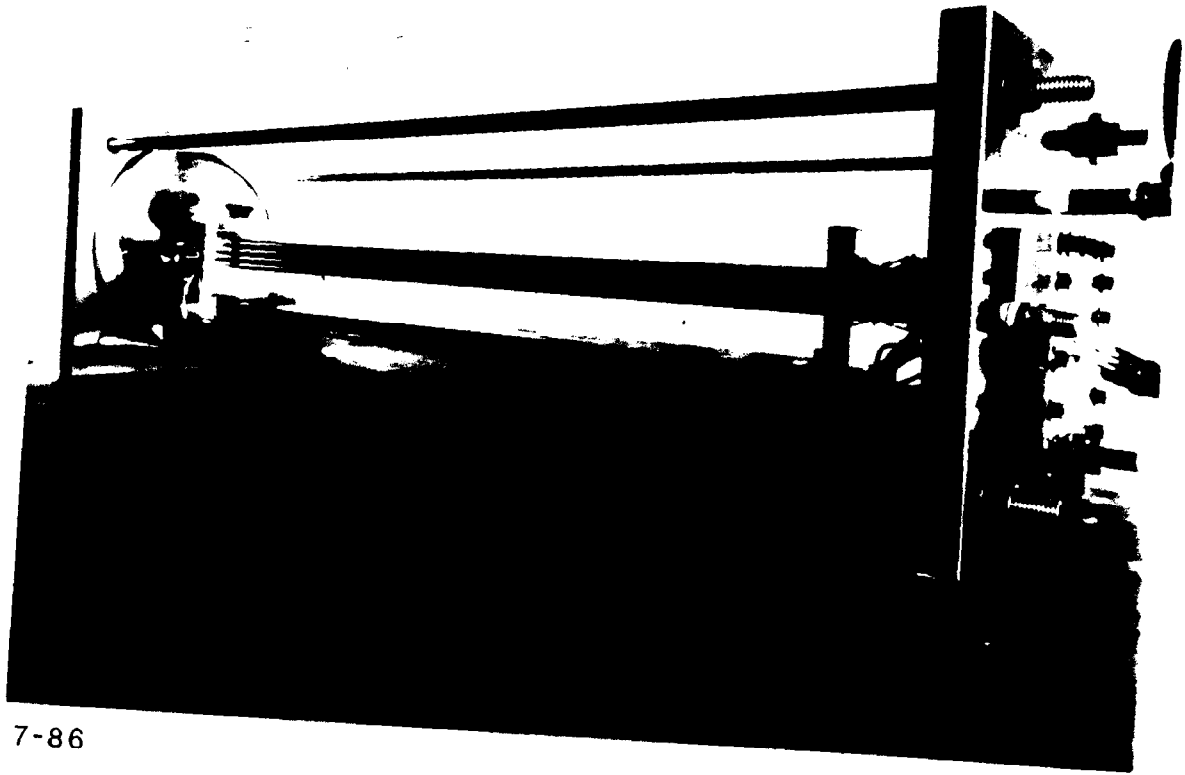
5625A3

Fig. 5



12-86

Fig. 6



7-86

5476A15

Fig. 7

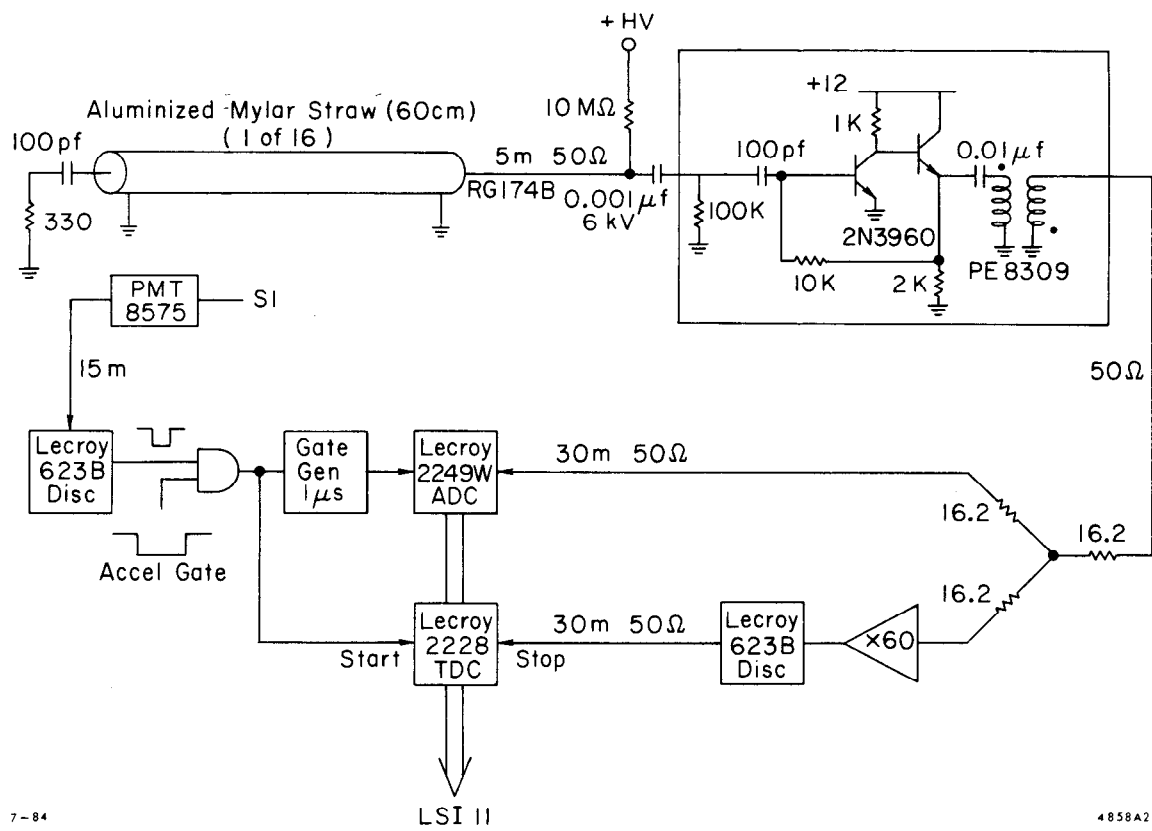


Fig. 8

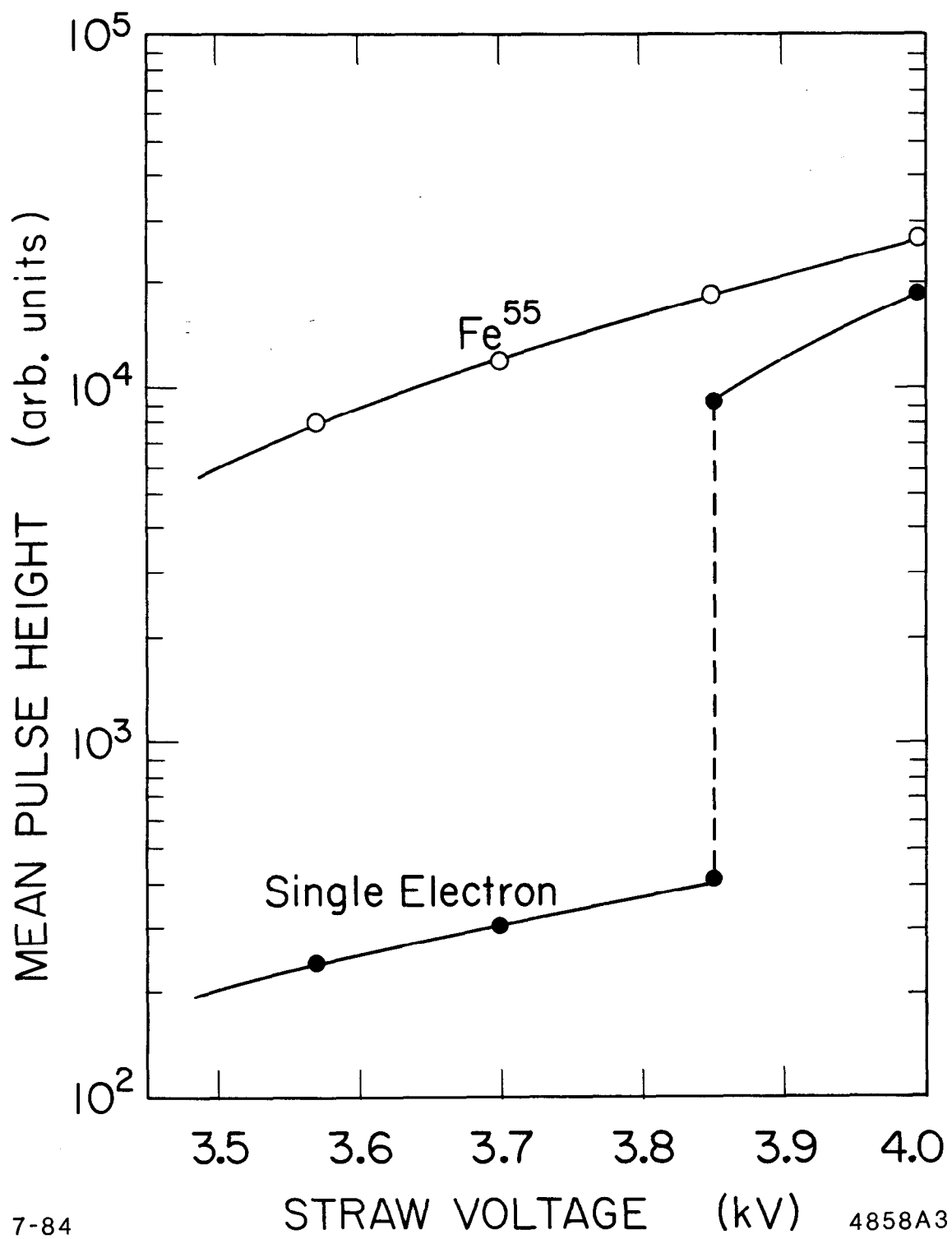
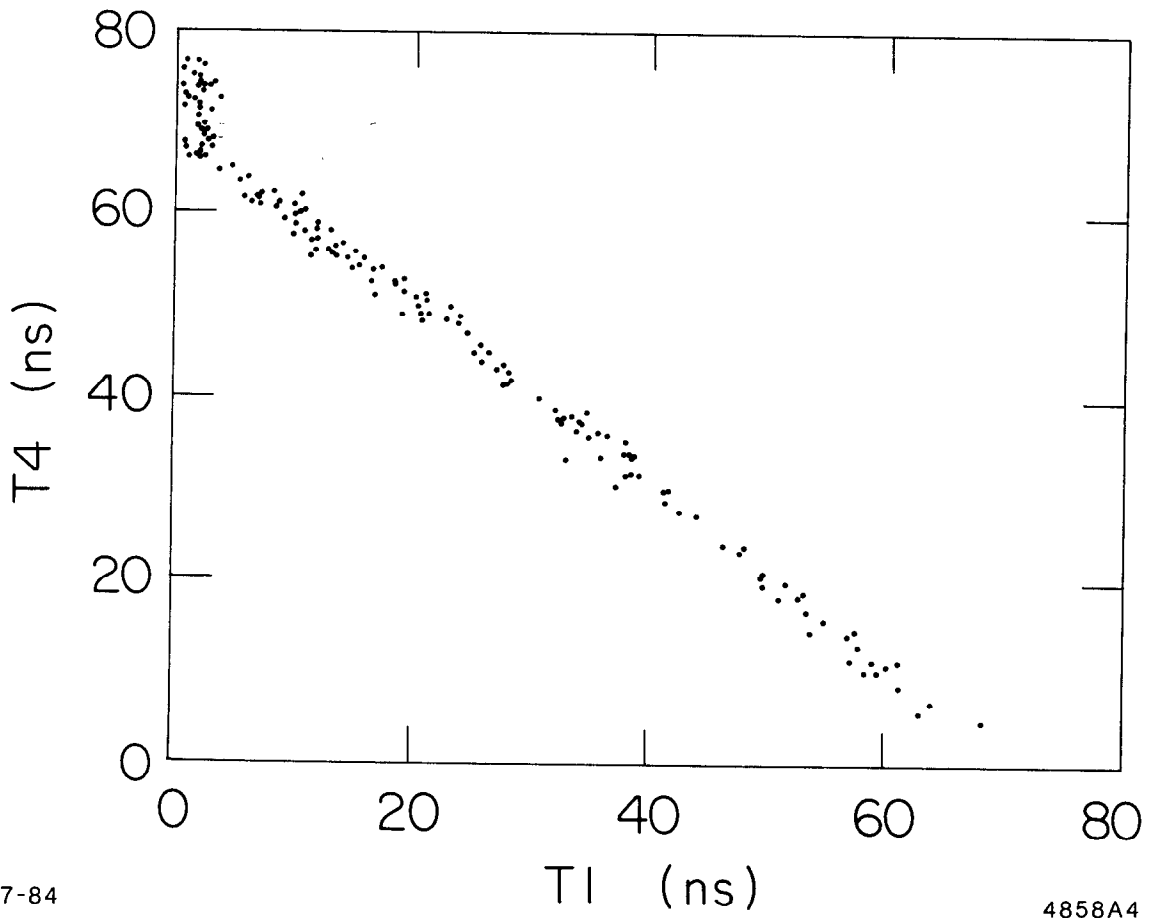


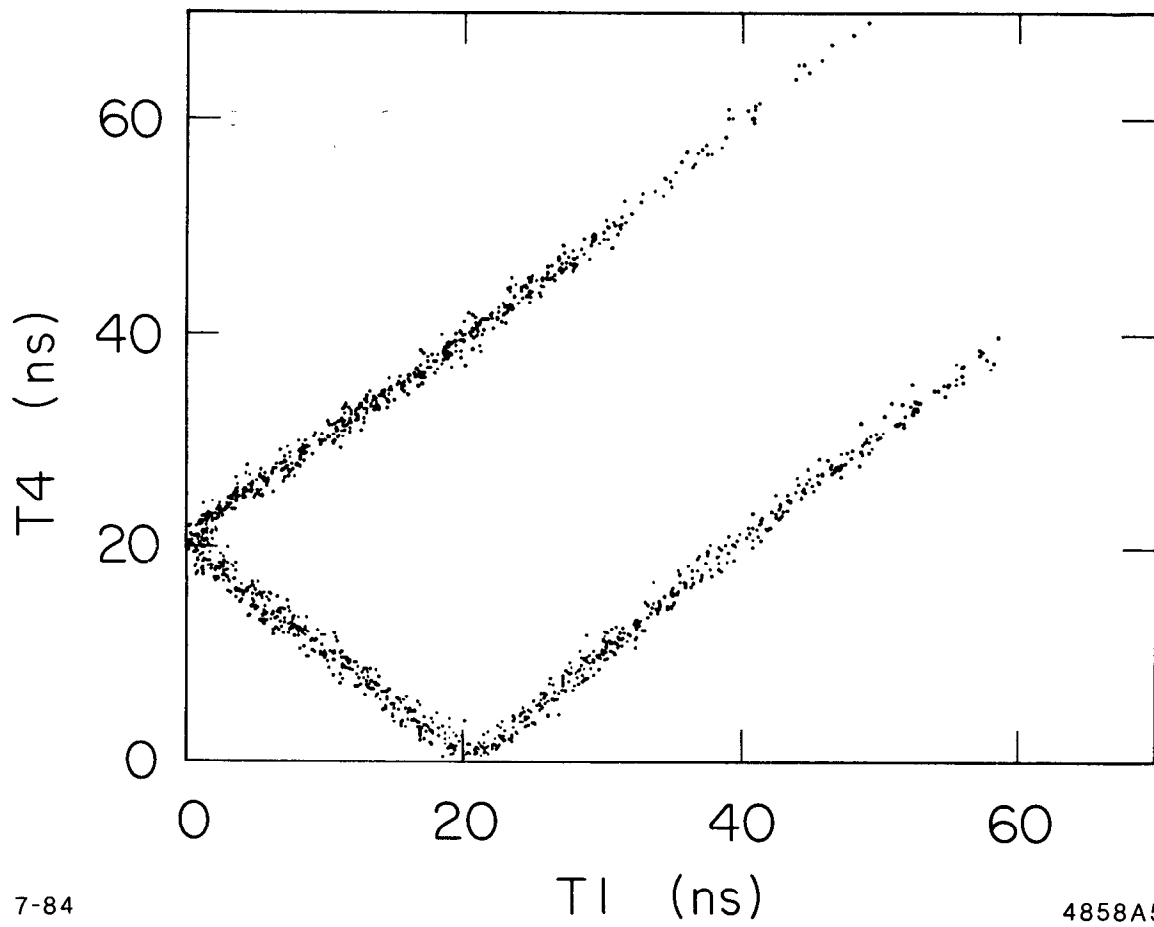
Fig. 9



7-84

4858A4

Fig. 10



7-84

4858A5

Fig. 11

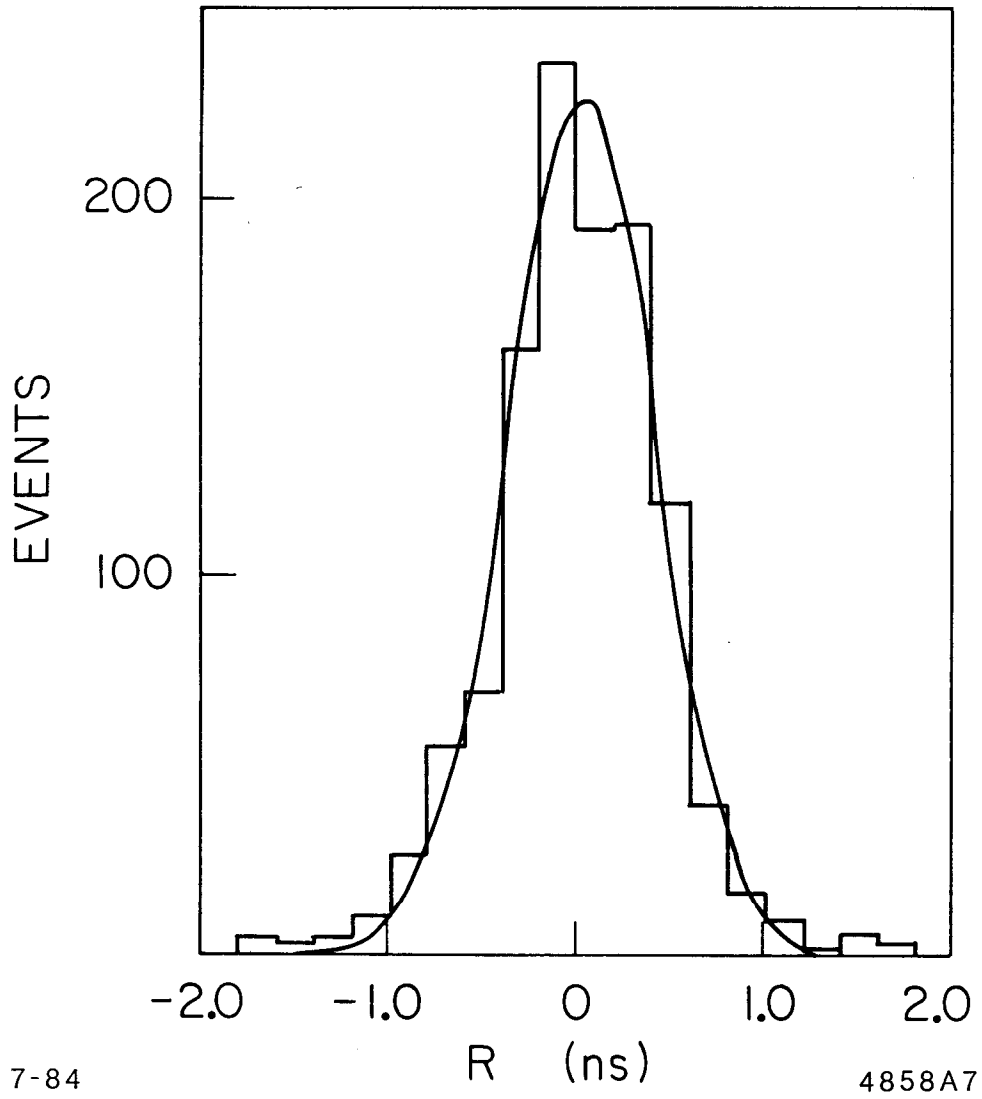


Fig. 12

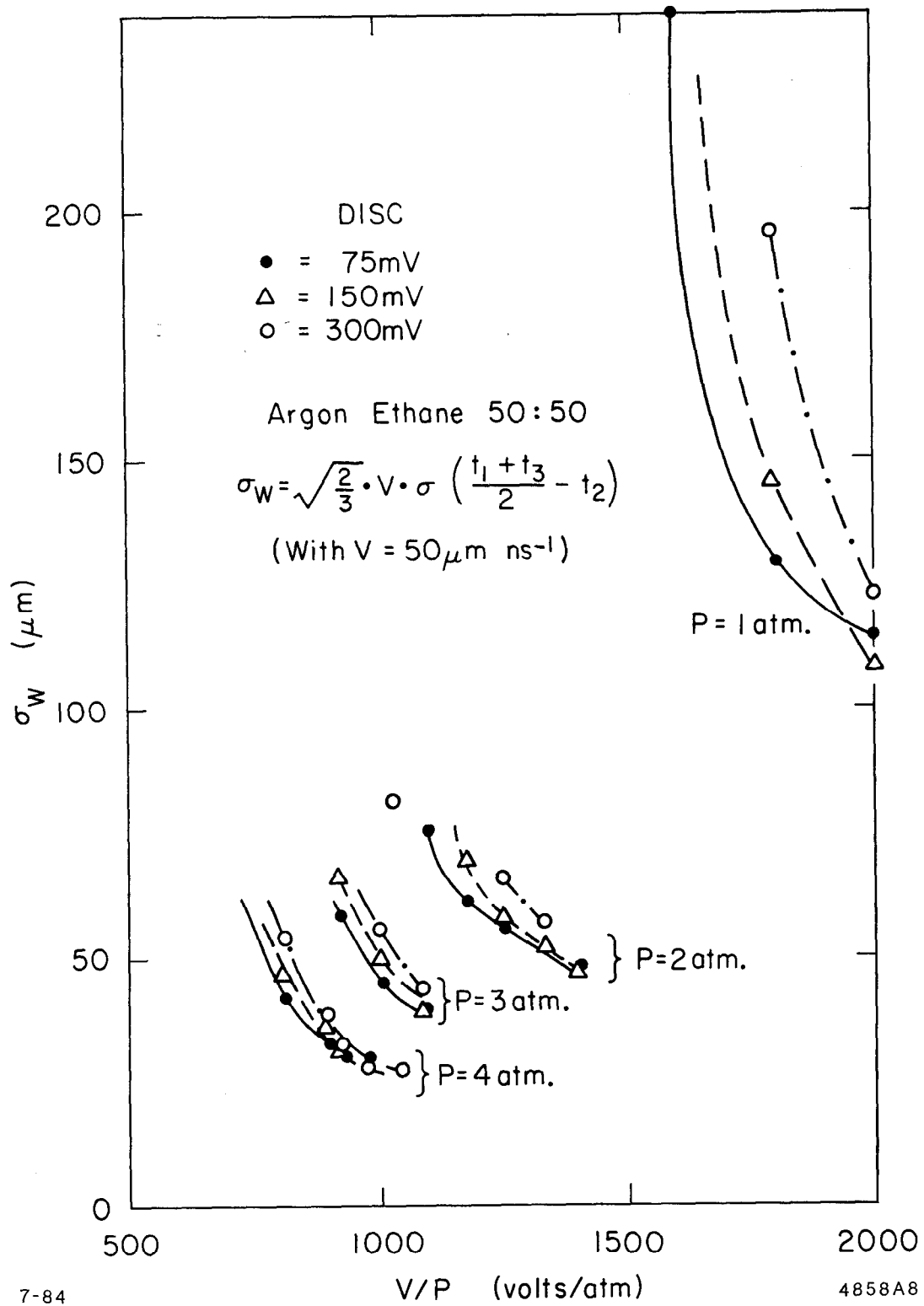


Fig. 13

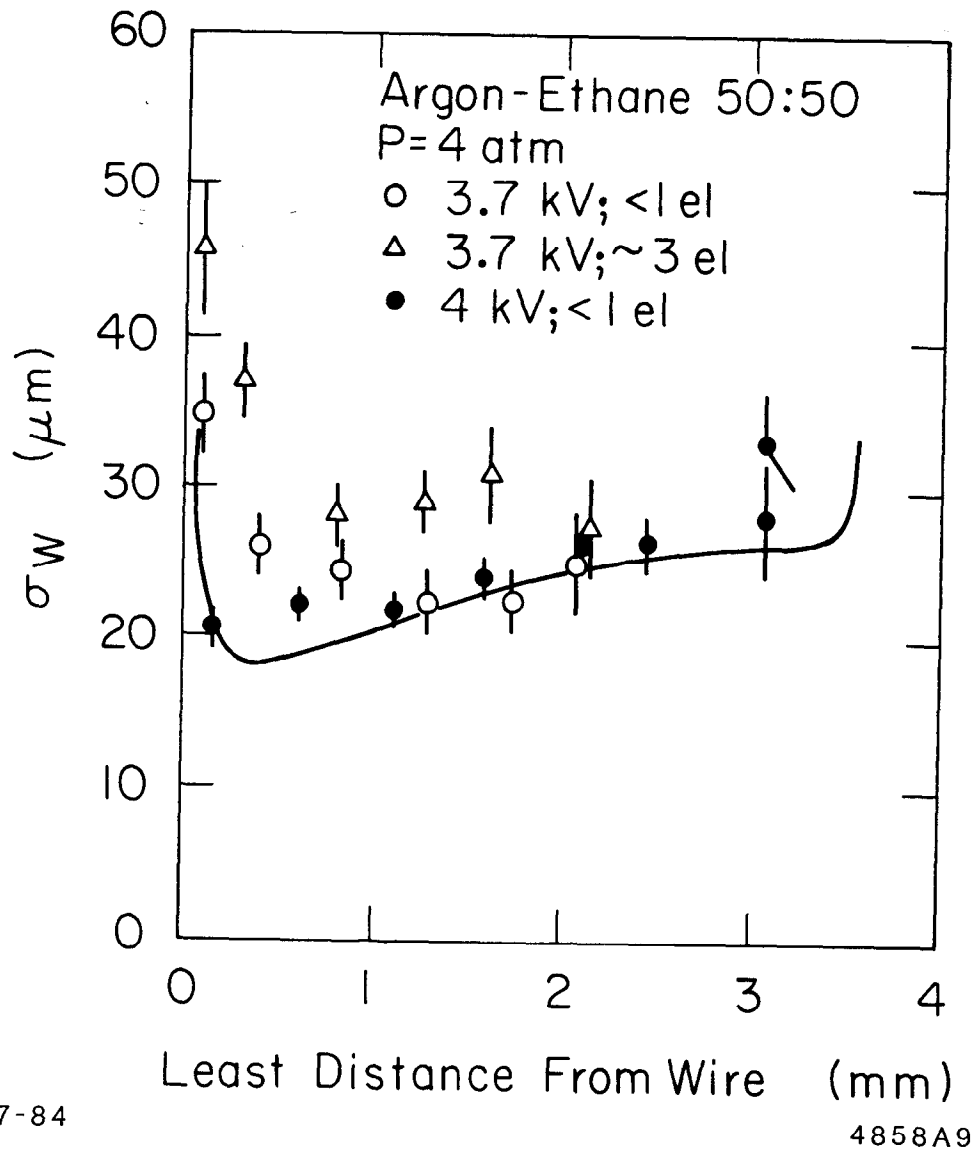


Fig. 14

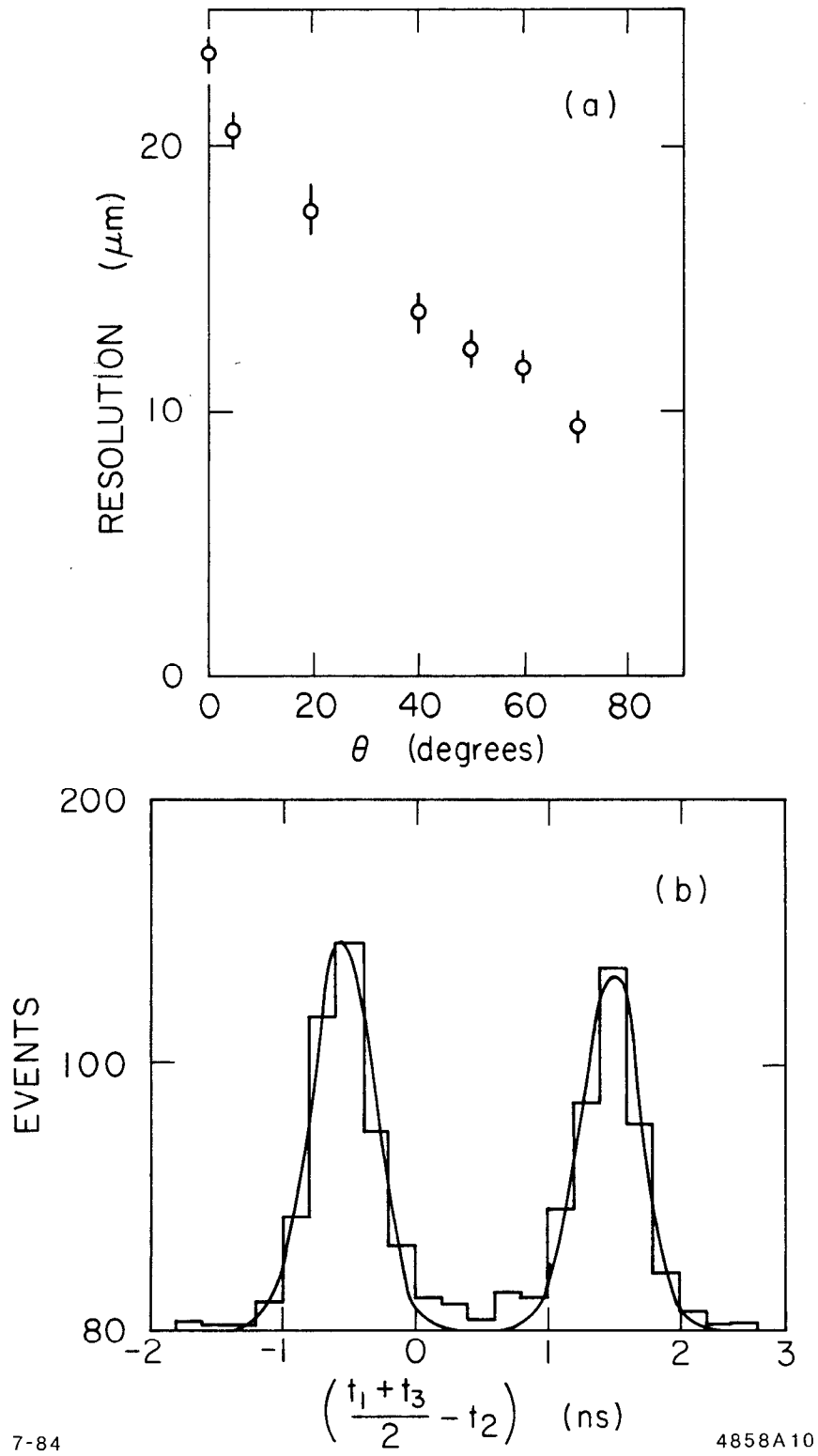


Fig. 15

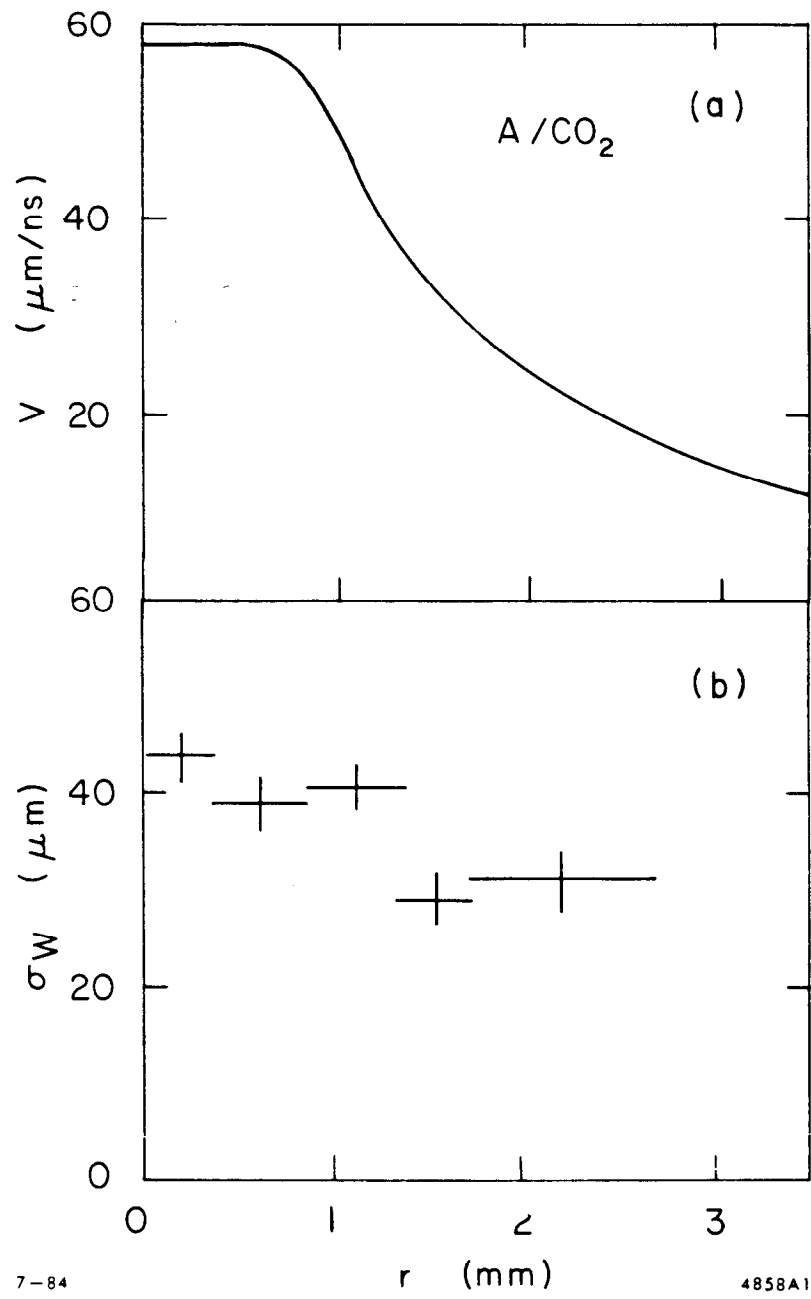
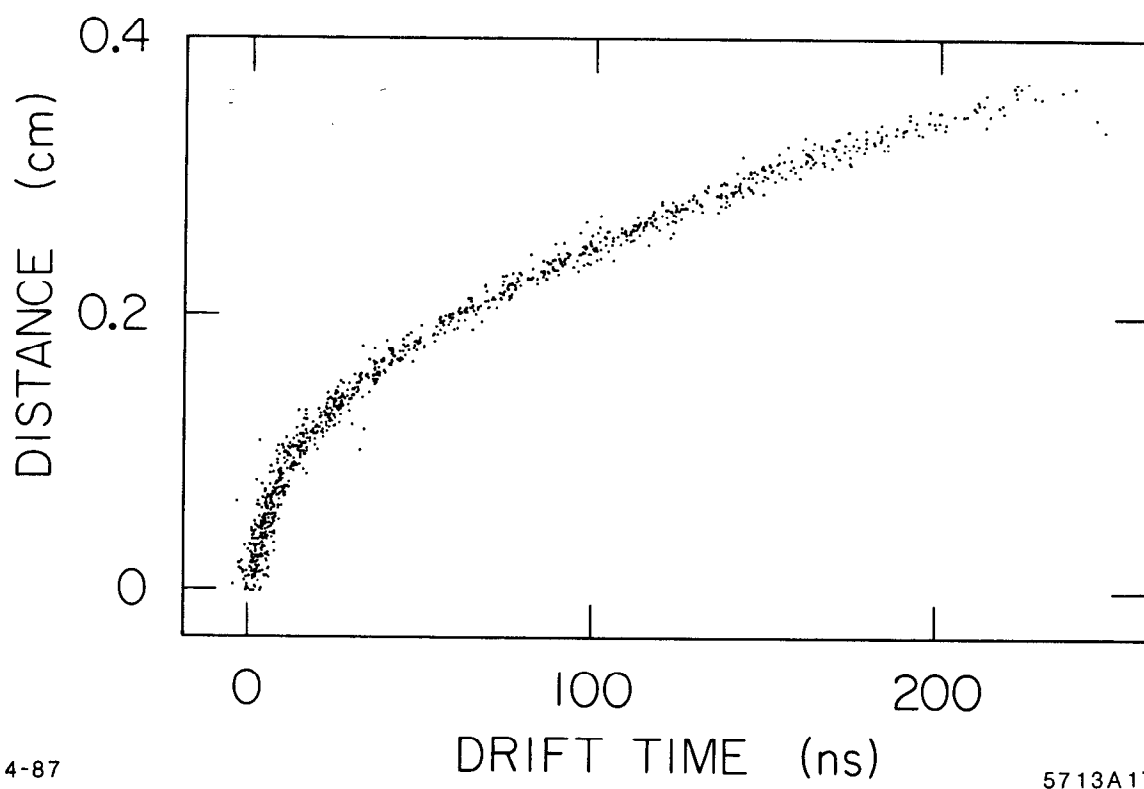


Fig. 16



4-87

5713A17

Fig. 17

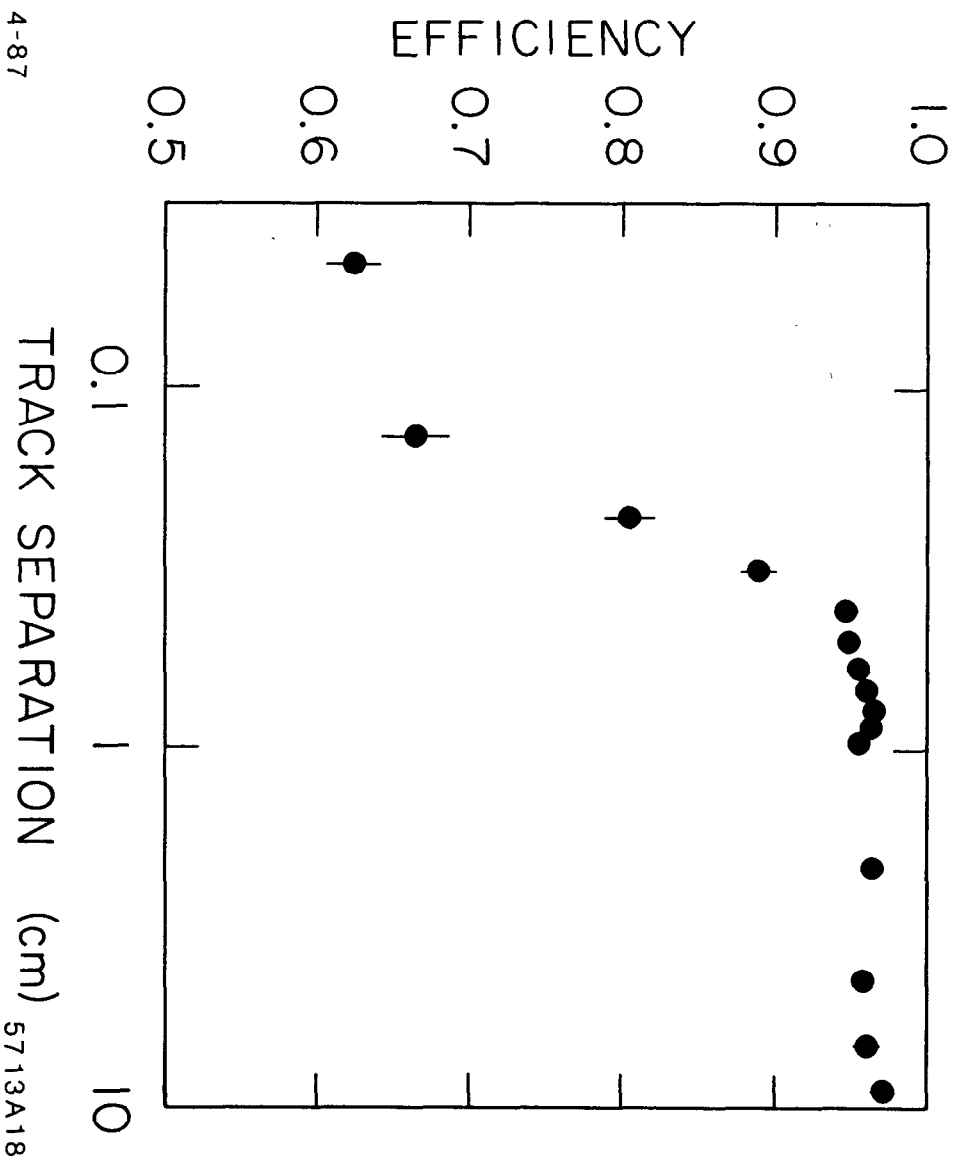
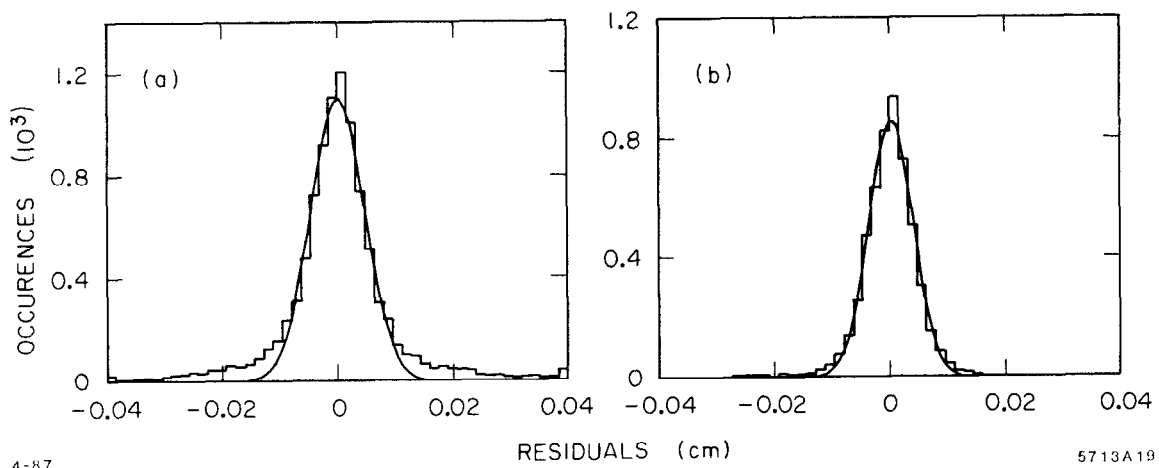


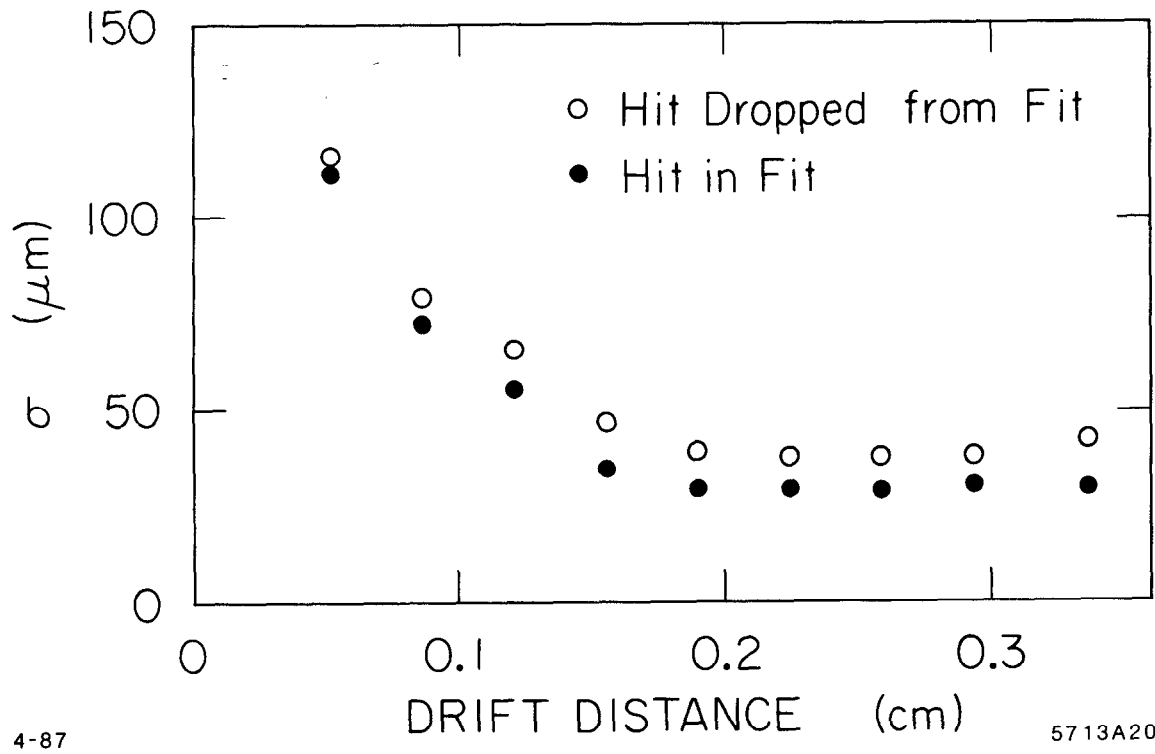
Fig. 18



4-87

5713A19

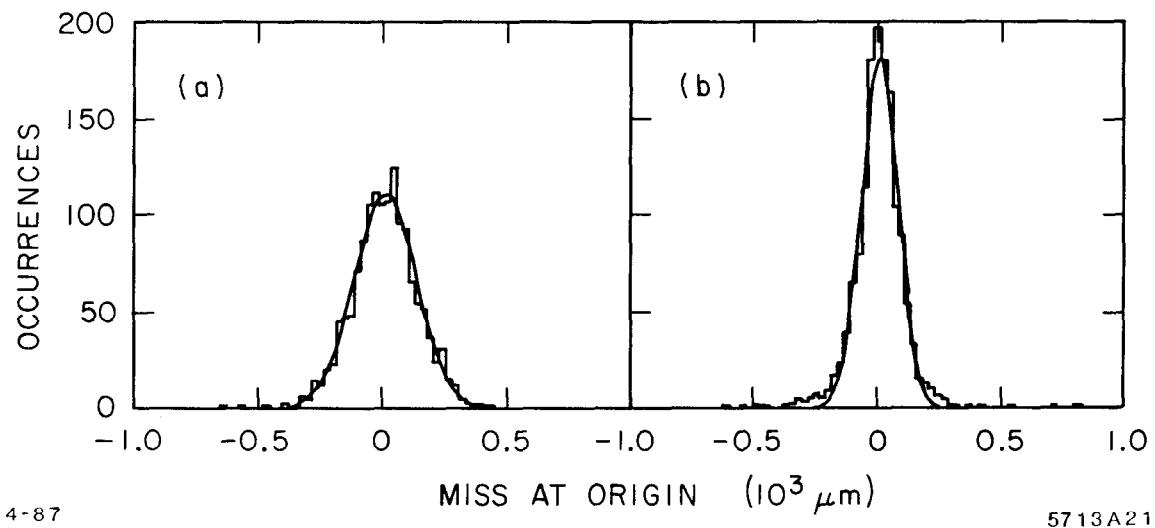
Fig. 19



4-87

5713A20

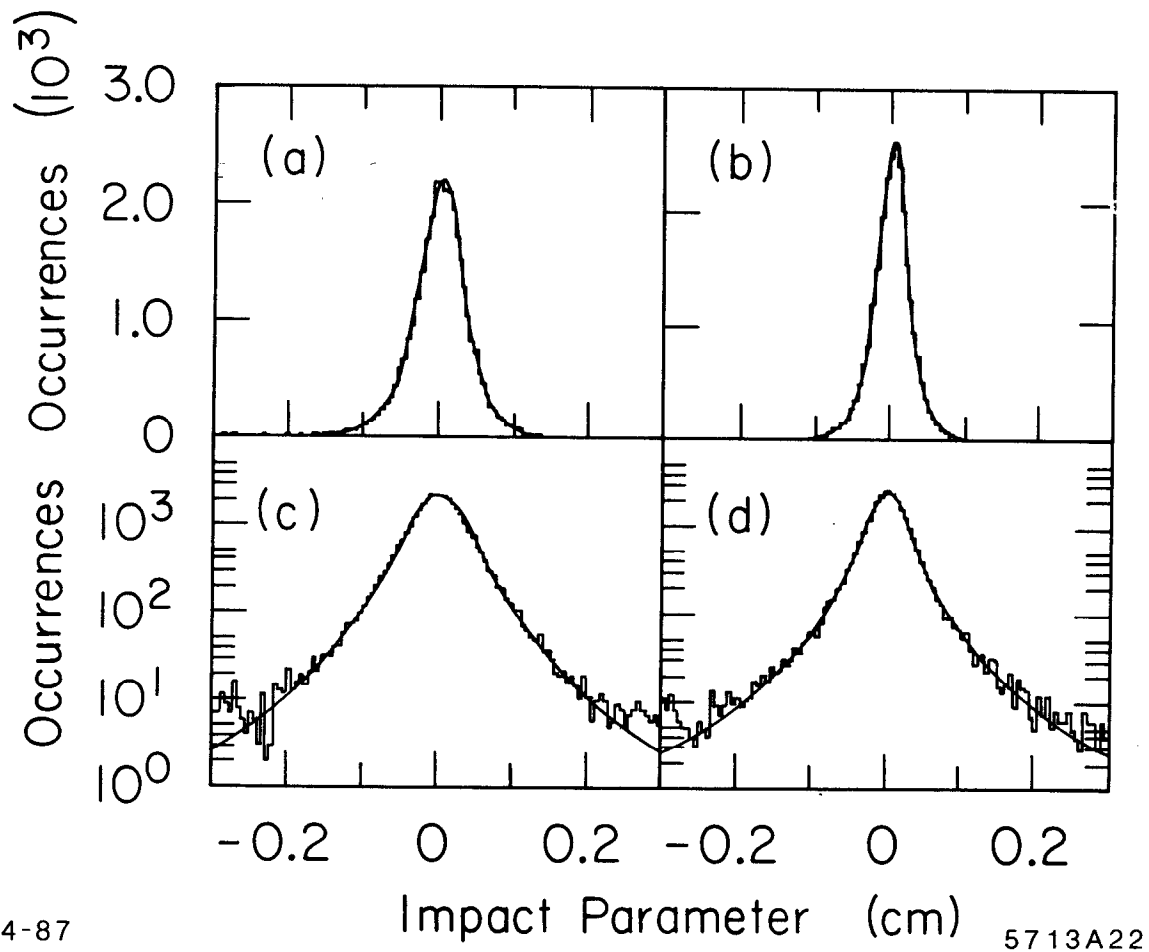
Fig. 20



4-87

5713A21

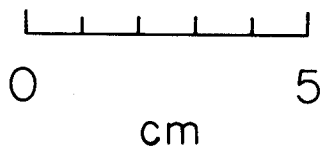
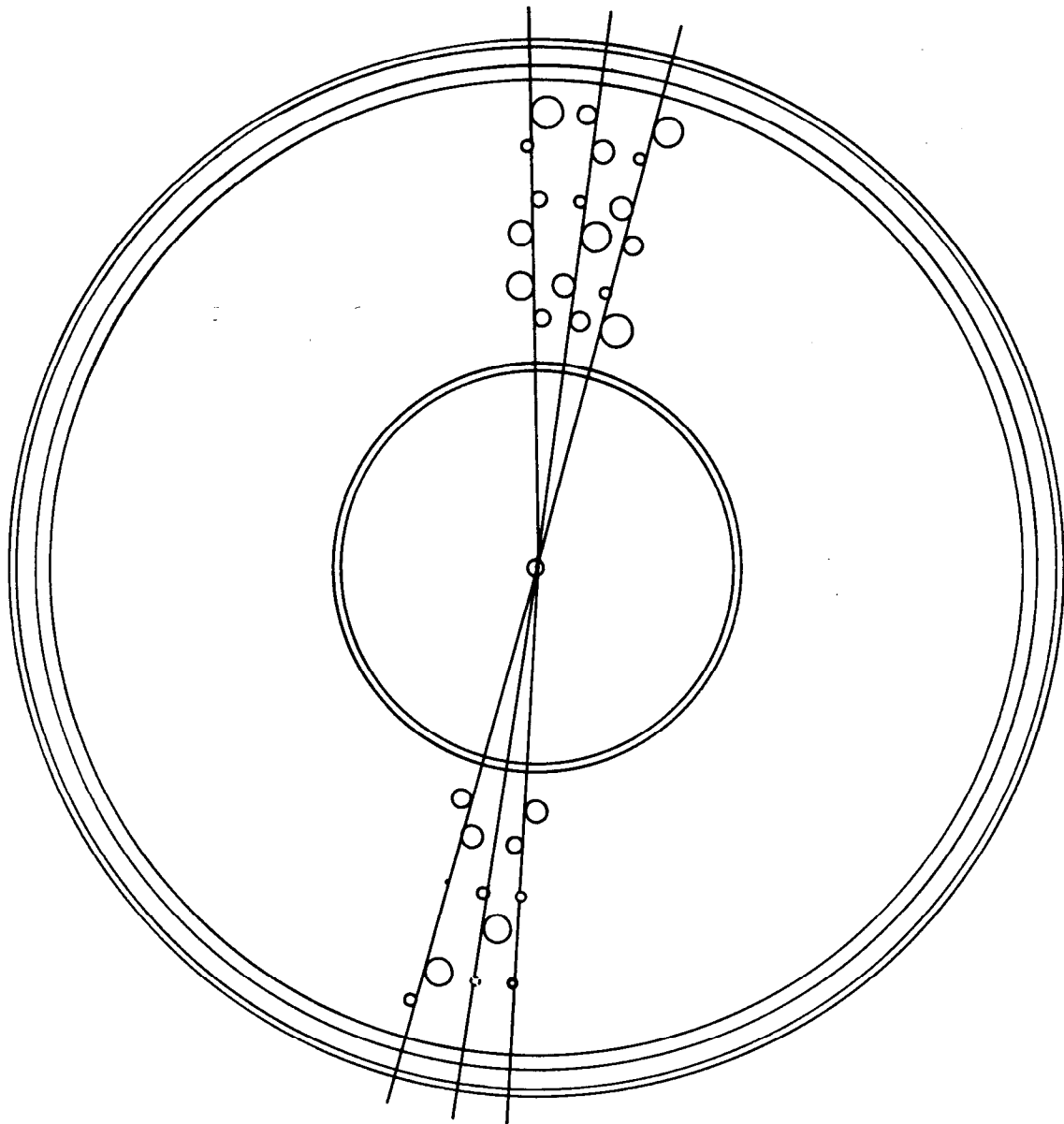
Fig. 21



4-87

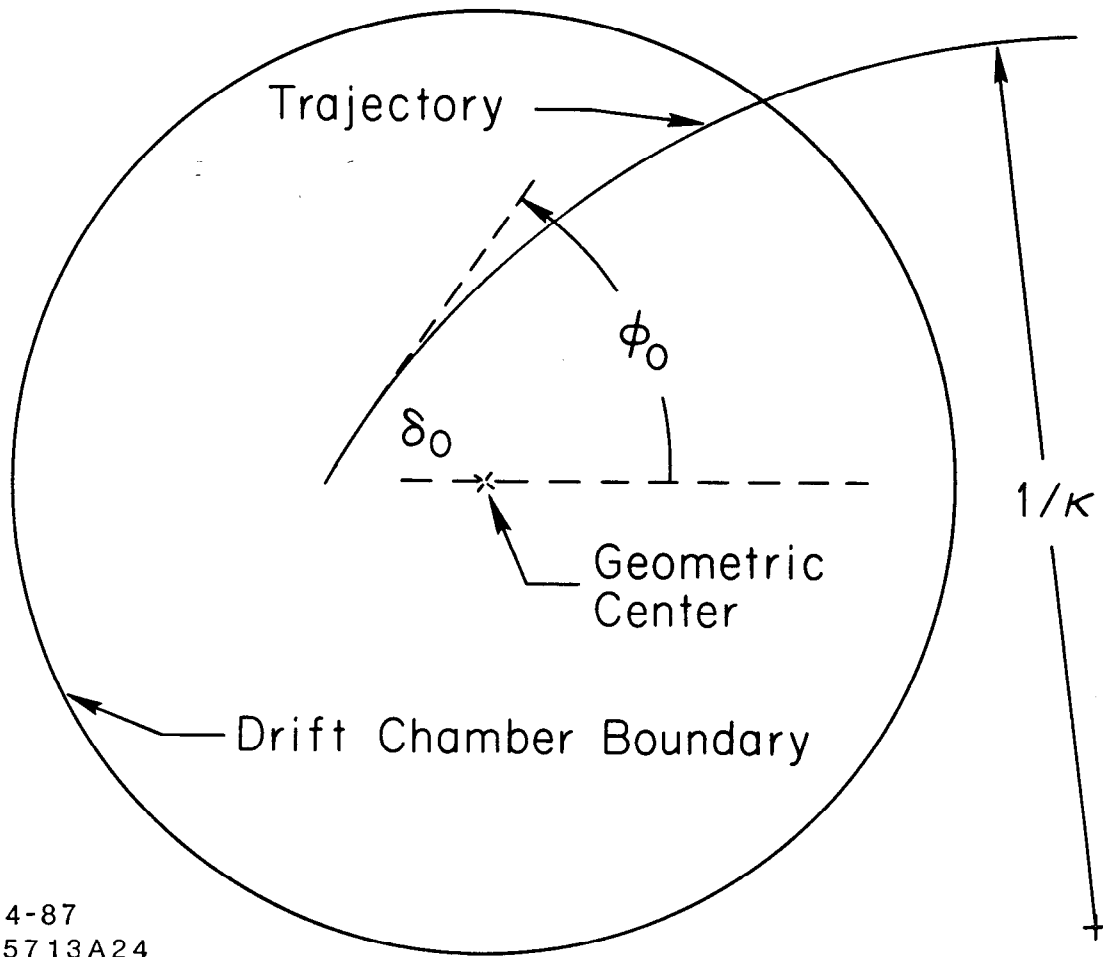
5713A22

Fig. 22



7-86
5476A14

Fig. 23



4-87
 5713A24

Fig. 24